Materials Today Advances 25 (2025) 100553

Contents lists available at ScienceDirect

Materials Today Advances

journal homepage: www.journals.elsevier.com/materials-today-advances/

Medium/high entropy alloys with heterogeneous structures for superior properties: A review

Yan Ma [a,1], Wei Wang [a,1], Jinyan He [b,**], Yuntian Zhu [c], Xiaolei Wu [a,d], Fuping Yuan [a,d,*]

[a] State Key Laboratory of Nonlinear Mechanics, Institute of Mechanics, Chinese Academy of Sciences, Beijing, China
[b] State Key Laboratory of NBC Protection for Civilian, Beijing, China
[c] Department of Materials Science and Engineering, City University of Hong Kong, Hong Kong, China
[d] School of Engineering Science, University of Chinese Academy of Sciences, Beijing, China

ARTICLE INFO

Keywords:
Heterogeneous structure
High-entropy alloy
Mechanical properties
Strain hardening
Hetero-deformation induced hardening
Magnet

ABSTRACT

Heterogeneous structures, such as gradient, lamellar, and dual-phase configurations, have been prevalent in nature for ages and have been harnessed in diverse applications to achieve exceptional properties in man-made engineering materials. These heterogeneous structures not only enhance the mechanical properties of the structured material but also exhibit immense potential in functional materials, enabling unprecedented functionalities. High entropy alloys (HEAs), a cutting-edge alloy design concept centered on multi-principal elements, offer a vast compositional landscape. The integration of HEA with heterogeneous structures further broadens the prospects for discovering new materials with remarkable attributes. This review delves into several types of heterogeneous structures within HEAs, highlighting their superior mechanical and functional properties, including strength, ductility, dynamic shear toughness, fracture toughness, fatigue properties, and magnetic capabilities. Additionally, it explores their deformation mechanisms and strain-hardening capabilities. This article provides a comprehensive overview of heterogeneous structured HEA for achieving enhanced mechanical and functional performance.

1. Introduction

Heterogeneous structures have existed ubiquitously in nature for a long history and have also been used in many areas to achieve superior properties by man-made engineering materials. While, the definition of heterogeneous materials was not fully clear, and the mechanical/physical properties of heterogeneous materials were not systematically studied by scientists until recently [1–4]. Heterogeneous materials were considered as a new class of materials in the last decade and were defined as materials with heterogeneous zones/domains with dramatically different (>100 %) mechanical/physical properties [5–7]. The integrated properties of heterogeneous materials are generally higher than those predicted by the rule-of-mixture, due to the synergistic effects generated by the interaction and coupling among these heterogeneous zones/domains [8–15]. Thus, heterogeneous materials generally possess unprecedented mechanical/physical properties that can't be achieved by their conventional homogeneous counterparts [16–18]. More importantly, heterogeneous materials can be easily fabricated utilizing common industrial facilities with very low costs such that their commercialization could be much easier as compared to the other advanced materials [16,19].

Heterogeneous materials have been quickly emerging as an important scientific research field recently due to their unprecedented properties and great potential for applications [20,21]. For example, heterogeneous structures have been implemented into medium/high entropy alloys (MEAs/HEAs) for obtaining excellent synergy of strength and ductility recently [22,23]. MEAs/HEAs have also emerged in the last two decades as a new class of materials [24–29]. MEAs/HEAs, also named multi-principle element alloys, typically containing three or more elements with equal or near equal molar ratio, show excellent mechanical properties due to the effects of high entropy, lattice distortion, sluggish diffusion, and chemical short-range order [30–33].

Since the first results were published in 2004 [26,27], HEA have evolved into a vast domain encompassing an extensive array of novel

* Corresponding author. State Key Laboratory of Nonlinear Mechanics, Institute of Mechanics, Chinese Academy of Sciences, Beijing, China.
** Corresponding author.
E-mail addresses: hejinyanfhy@163.com (J. He), fpyuan@lnm.imech.ac.cn (F. Yuan).
[1] These authors contributed equally.

https://doi.org/10.1016/j.mtadv.2024.100553
Received 26 September 2024; Received in revised form 19 December 2024; Accepted 21 December 2024
Available online 28 December 2024

alloy systems. This class of materials encompasses various subclasses, including Face-Centered Cubic (FCC) single-phase HEAs, dual-phase HEAs, eutectic HEAs with an FCC matrix, and refractory HEAs characterized by a Body-Centered Cubic (BCC) matrix, each exhibiting distinct physical properties. Specifically, FCC HEAs are typically distinguished by their high fracture toughness at cryogenic temperatures [24–29]. Conversely, refractory HEAs generally exhibit exceptional structural stability, leading to superior performance at elevated temperatures [24–29].

Combination of heterogeneous structures and MEAs/HEAs can give us an opportunity to achieve even better properties [16,20]. Thus, the objective of this review paper is to introduce the MEAs/HEAs with heterogeneous structures to the materials research community, particularly the types of heterogeneous microstructures, the processing technologies, their mechanical/physical properties, and their potential applications.

2. Types of heterogeneous structures

Based on the application purposes, heterogeneous materials can be differentiated into two types of different categories: heterogeneous structural materials and heterogeneous functional materials. Heterogeneous structural materials and heterogeneous functional materials are defined by various domains with dramatic differences in mechanical properties or physical properties, respectively [5,34]. Conventional materials might also contain heterogeneous domains to some extent, such as relatively inhomogeneous grain size distribution, and multiple phases, while the typical indicator of heterogeneous materials is the strong synergistic effects above the rule of mixture in mechanical properties or physical properties due to the dramatic difference of microstructures in various domains [4,6,35]. Since most reports have been focused on heterogeneous structural materials so far in the literature, thus the main part of this review will emphasize the heterogeneous structural materials and heterogeneous functional materials will only be discussed briefly in the later section.

The conventional methods for fabricating heterostructures can be categorized into four distinct approaches: Surface Mechanical Attrition Treatment (SMAT), Rolling and Annealing (RA), Accumulative Roll Bonding (ARB), and Mechanical Milling of Powder Metallurgy (MMPM) [1–5]. SMAT is predominantly utilized for the creation of gradient structures [36–38],. The RA technique is employed to process heterogeneous grain structures [39–41] and heterogeneous lamella structures [42,43]. The ARB method is specifically applied to fabricate laminate structures [44–46], which consist of alternating layers of two or more different materials [1]. Lastly, MMPM is employed to prepare harmonic structure [47–49] and bimodal [50–52], which are characterized by the harmonious integration of different material properties, or by the presence of two distinct populations of grains or phases respectively.

The illustration of various types of heterogeneous structures is displayed in Fig. 1. These types of heterogeneous structures can also be classified into three different categories: the first one is characterized by a distribution of heterogeneous grains or multiple phases with a relatively larger scale; the second one is defined by a distribution of heterogeneous sub-structures with a relatively smaller scale, such as nanotwins, nanoprecipitates, and dislocation cells/walls; lastly, the third one can be expressed as the dual-heterogeneous structures by the combination of the first two categories [6].

2.1. Gradient structures

The gradient structures generally refer to the structures with microstructural gradients along the depth, and the microstructural gradients can be from grain size, fraction of constituent phases, twin density, nanoprecipitate density, dislocation cell density or a

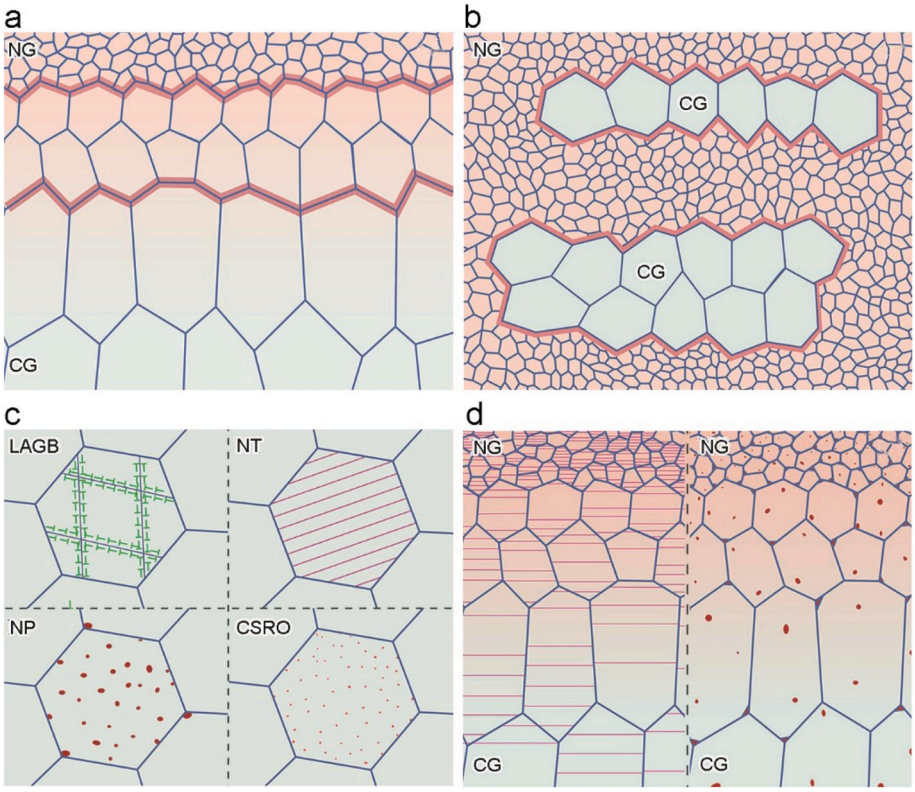

Fig. 1. The illustration of various types of heterogeneous structures. (a) Gradient structure. (b) Lamellar structure. (c) Sub-zone heterogeneous structures including low-angle grain boundary (LAGB), nano-twin (NT), nanoprecipitate (NP), and chemical short-range order (CSRO). (d) Multiple heterogeneous structures. Reproduced from Ref. [6].

combination of these microstructural units. Gradient structures have also been applied to MEAs/HEAs to achieve superior mechanical properties [53–55]. For example, gradient cell structures have been introduced into a stable FCC phase $Al_{0.1}CoCrFeNi$ HEA utilizing a cyclic-torsion treatment, by which spatially gradient plastic strains from the surface to the core can be imposed [55,56]. The detailed microstructure characterizations for this type of gradient cell structures are shown in Fig. 2. The gradient cell structure displays a sample-level hierarchical dislocation structure. The grain sizes defined by high-angle grain boundaries still show a relatively homogeneous distribution along the depth and random crystallographic orientations. However, a gradient in dislocation density along the depth is observed for this structure. The dislocation density is very low at the sample core although a typical planar single-slip dislocation configuration is observed, while extensive well-developed dislocation walls/cells with low-angle boundaries can be found at the topmost layer. Each cell wall with a thickness of about 40 nm is decorated with a high density of dislocations ($\sim 2 \times 10^{15}$ m^{-2}). It is also found that the misorientations for these cells have a range from 0.7 to 4.8°, indicating low-angle boundaries between these cells. Thus, the cell size, instead of grain size, is observed to increase with increasing depth for this gradient cell structure.

Structures with combined gradients (grain size and volume fraction of nanoprecipitates) have been designed and introduced into the $Al_{0.5}Cr_{0.9}FeNi_{2.5}V_{0.2}$ HEA [36,57]. The microstructure characterizations for the dual-graded structures are displayed in Fig. 3. Both densities of high-angle grain boundaries and low-angle grain boundaries show a decreasing gradient from the surface to the core, indicating gradient distributions for both grain sizes and dislocation cells. Moreover, the volume fraction of B2 nanoprecipitates is found to show a decreasing gradient from the surface to the core. It is also found that the relative volume fraction of coherent $L1_2$ nanoprecipitates is much higher at the topmost layer (64.2 %) than at the core layer (31.8 %), indicating a decreasing gradient along the depth for the volume fraction of the $L1_2$ phase. Thus, the hardness gradient for this dual-graded structure can be due to the combined gradients for densities of grain boundaries, and volume fractions for both B2 and $L1_2$ nanoprecipitates along the depth.

2.2. Heterogeneous grain structures

One of the earliest reported heterogeneous structures is bi-modal or multi-modal grain structures, in which the grain size distributions have two or multiple peaks [58,59]. These bi-modal or multi-modal grain structures generally have a wide range of grain size (from several tens of nanometers to several hundreds of micrometers), and they are usually produced by cold rolling followed by annealing at critical temperatures. This strategy for heterogeneous grain structures was initially applied to Al alloys [60,61], pure copper [58,62], pure nickel [59], and titanium alloys [63,64]. More recently, heterogeneous grain structures have also been applied to the M/HEAs [39,40]. For example, a three-level heterogeneous grain structure has been also deployed in CrCoNi MEA to achieve gigapascal-level yield strength along with appreciable tensile ductility. This heterogeneous grain structure is obtained by partial recrystallization annealing following conventional cold rolling (as displayed in Fig. 4a). The partial recrystallization results in a heterogeneous grain structure that is characterized by three levels of grains with obviously different grain sizes, i.e., the largest micro-grains with a mean grain size of 2.3 μm, the intermediate ultrafine-grains with grain size range from 250 nm to 1 μm, and the smallest nanograins with grain size less than 250 nm [39]. It is interesting to note that almost all nanograins are in the locations of grain boundaries and triple junctions of ultrafine grains, such an arrangement should be expected due to the low stacking fault energy for this MEA. As indicated by the TEM image (Fig. 4b), a twinned nanograin is located in the vicinity of the high-angle grain boundary of its parent grain, and such twinned grains should often be called corner twins [65,66]. Actually, the formation of corner twins by discontinuous nucleation for recrystallization is a well-known mechanism for metals with low stacking fault energy. The three-level heterogeneous grain structure can impart an excellent synergy of yield strength and tensile ductility in the MEAs/HEAs, as discussed in the later

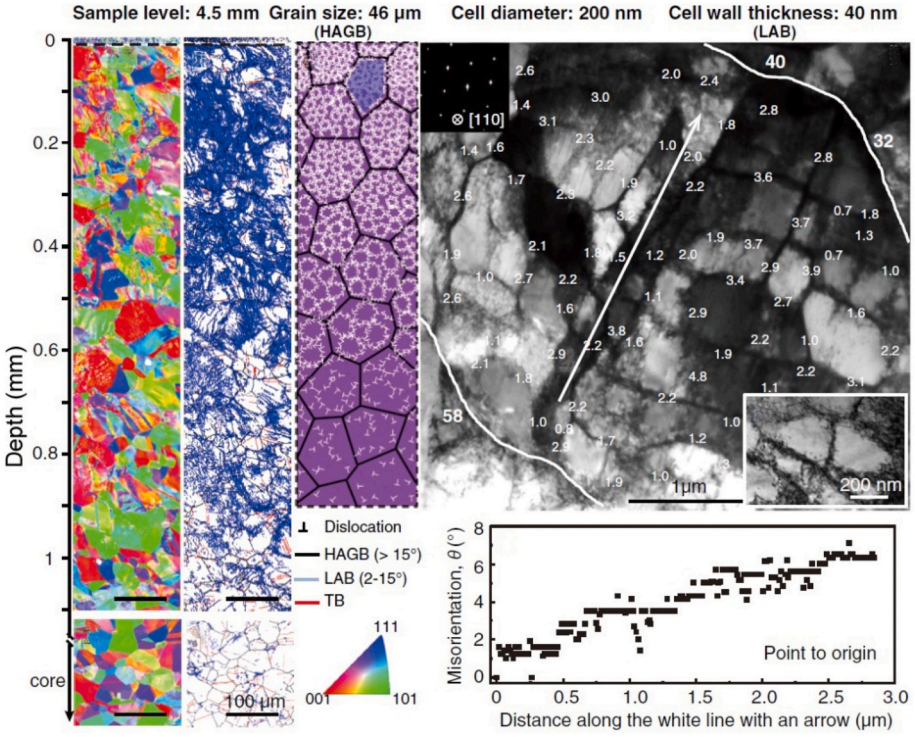

Fig. 2. Microstructure characterizations for the gradient cell structure in the $Al_{0.1}CoCrFeNi$ HEA. The numbers in the TEM image are the misorientation angle of each cell wall. Reproduced from Ref. [55].

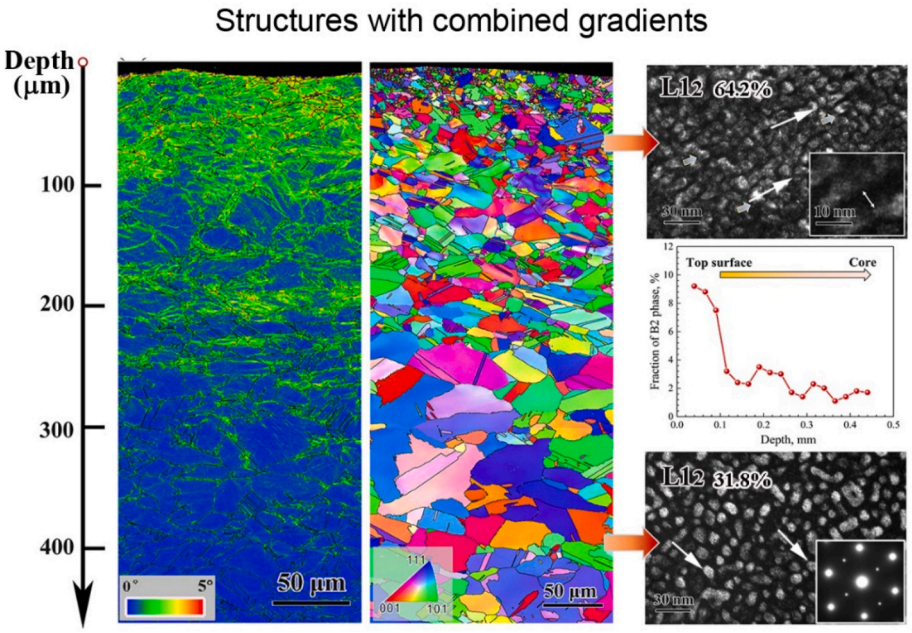

Fig. 3. Dual-gradient structures in the $Al_{0.5}Cr_{0.9}FeNi_{2.5}V_{0.2}$ HEA. Reproduced from Ref. [36].

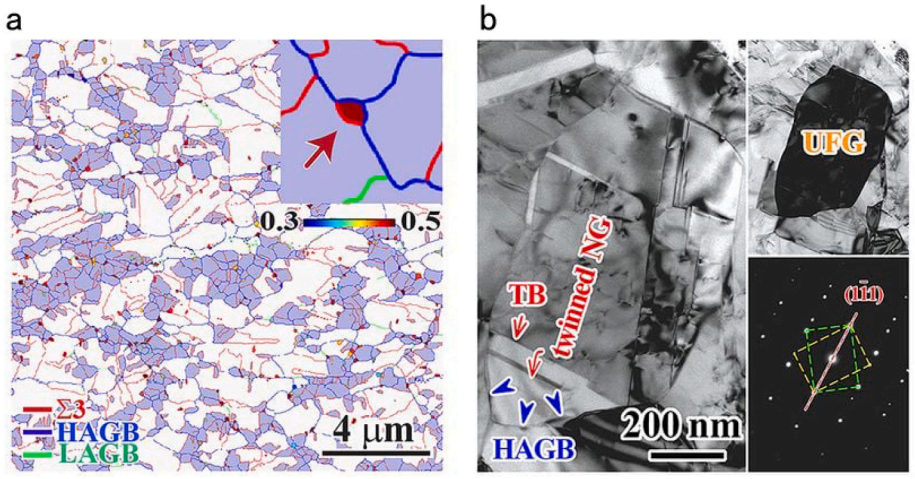

Fig. 4. A three-level heterogeneous grain structure in the CrCoNi MEA. (a) EBSD grain boundary image showing three grades of grain size. (b) TEM image showing a twinned nano grain at the lower part of an ultra-fined grain (UFG). Reproduced from Ref. [39].

sections.

A dual heterogeneous structure with both heterogeneous grain structure and coherent nanoprecipitates has been deployed in the $(CrCoNi)Al_3Ti_3$ MEA by carefully controlled alloy composition and critical thermomechanical processing, obtaining both ultrahigh strength and large uniform elongation [67]. This dual heterogeneous structure is displayed in Fig. 5. Microstructure characterizations reveal a heterogeneous grain matrix with both coarse grains and ultrafine grains. The high density of annealing twins and stacking faults can be found in the matrix. Moreover, coherent $L1_2$ nanoprecipitates can be found in both coarse grains and ultrafine grains. The size of coherent $L1_2$ nanoprecipitates is less than 5 nm, and the volume fraction of the coherent $L1_2$ phase is very high. Many similar dual heterogeneous structures have also been applied to the other MEAs/HEAs to achieve better mechanical properties [68–70].

2.3. Dual-phase or multiple-phase structures

Structures consisting of two or more phases with different crystal structure or chemical compositions can be called as dual-phase or multiple-phase structures [50,71]. Conventional eutectic structures are one of dual-phase structures with different crystal structures [72], while spinodal decomposition structures are one of dual-phase structures with the same crystal structures but different compositions [73]. Dual-phase or multiple-phase structures can also be considered as a class of heterogeneous structures since the mechanical properties of different phases are dramatically different in general. Significantly, stress/strain partitioning plays an important role during tensile deformation for achieving excellent tensile properties. Recently, the strategy of dual-phase or multiple-phase structures has also been applied to the MEAs/HEAs [74–76]. For example, a dual-phase structure has been produced in the $Fe_{80-x}Mn_xCo_{10}Cr_{10}$ (x = 45 at%, 40 at%, 35 at% and 30 at%) HEAs by relaxing the strict restrictions on equal-molar or near equal-molar compositions for HEAs [50], since HEAs were originally

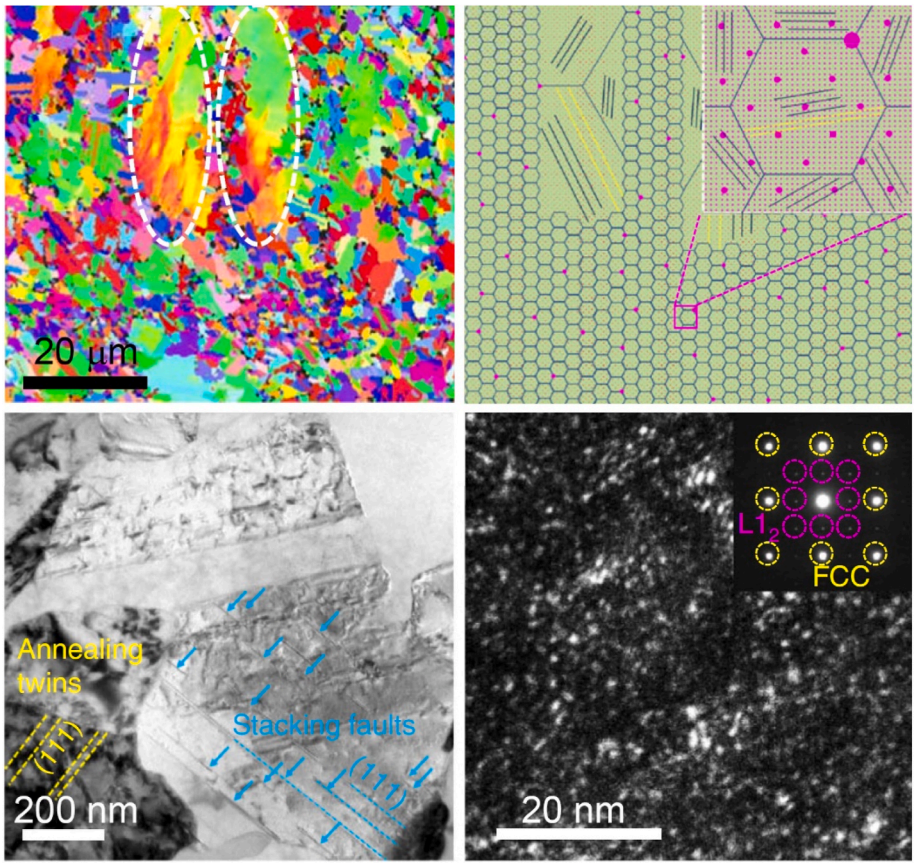

Fig. 5. A dual heterogeneous structures with both heterogeneous grain structure and coherent nanoprecipitates in the (CrCoNi)Al_3Ti_3 MEA. Reproduced from Ref. [67].

designed to generate single-phase solid-solution benefitted from phase stabilization through entropy maximization [77,78]. The dual-phase structure with both FCC and HCP phases in the $Fe_{80-x}Mn_xCo_{10}Cr_{10}$ HEA is displayed in Fig. 6. The reduced phase stability in this dual-phase HEA can result in two benefits: interface strengthening/hardening from the dual-phase structure, and strong strain hardening from the

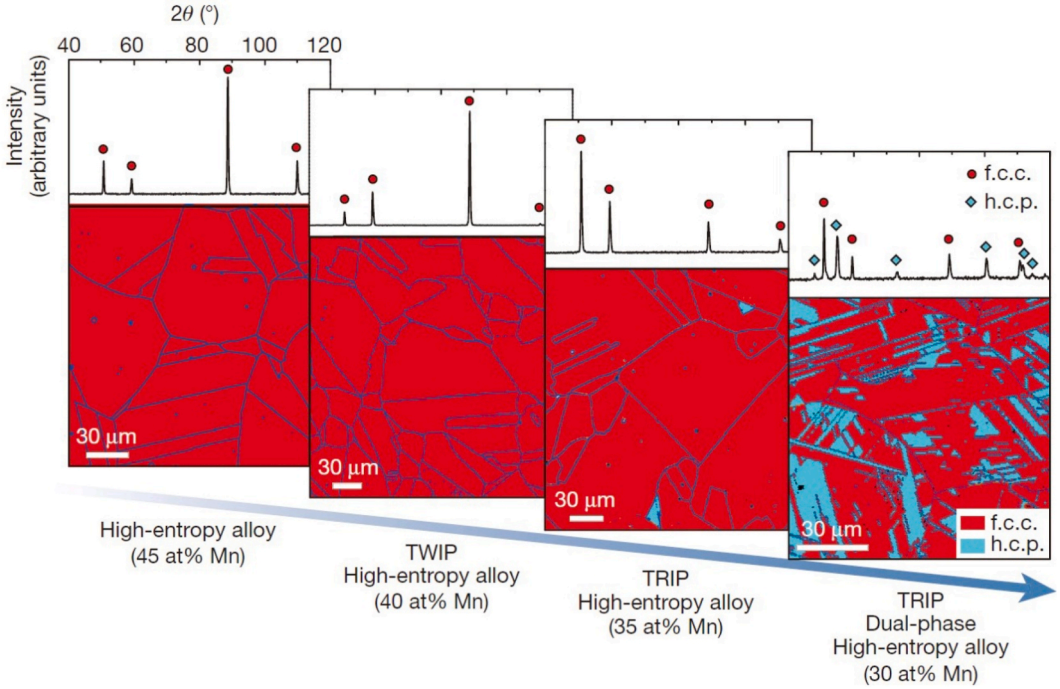

Fig. 6. A dual-phase structure in the $Fe_{80-x}Mn_xCo_{10}Cr_{10}$ (x = 45 at%, 40 at%, 35 at% and 30 at%) HEAs. Reproduced from Ref. [50].

transformation-induced-plasticity (TRIP) effect. The HCP phase in this dual-phase structure is formed due to the partial martensitic transformation from the FCC crystal structure to the HCP crystal structure upon cooling from the high-temperature single-phase region by decreasing the Mn content in the $Fe_{80-x}Mn_xCo_{10}Cr_{10}$ HEAs [50].

Conventional eutectic structures have also been designed and deployed into the $Al_{19}Fe_{20}Co_{20}Ni_{41}$ HEA to obtain much larger tensile ductility through hierarchical crack buffering [51]. The eutectic structures with both the harder B2 phase and softer $L1_2$ phase in the $Al_{19}Fe_{20}Co_{20}Ni_{41}$ HEA are shown in Fig. 7. Two totally different microstructures are obtained by two different methods, conventional casting and directional solidification [51]. The former method generates a typical lamellar eutectic microstructure with various growth directions in varying equiaxed grains, as indicated in Fig. 7a–c. While, a hierarchical eutectic structure is produced by the second method, directional solidification, as shown in Fig. 7d–f. There are two different scale levels of hierarchy existing in this structure. First, two different kinds of columnar grains are aligned along the directional solidification direction, softer aligned (grain center) and harder branched (rims of the grains) eutectic colonies at the large scale. Second, each colony contains soft $L1_2$ and hard B2 lamellae at the small scale. This bone-like hierarchical eutectic structure has significant advantages to buffer cracks for achieving high uniform elongation [51].

2.4. Chemical short/medium-range order

The aforementioned heterogeneous structures generally contain microstructures with varying length scales from several nanometers to several hundreds of micrometers. While, a new type of microstructure at even smaller length scale has been revealed recently for MEAs/HEAs, i.e., chemical short-range order (CSRO) or chemical medium-range order (CMRO) [79–83]. In general, MEAs/HEAs with high configurational entropy are assumed as an ideal solution, while the enthalpic interactions among composed elements are also expected to result in various degrees of local chemical ordering [84,85]. These local chemical ordering is generally accompanied with the element re-distributions at the atomic scale [86]. The CSRO in VCoNi MEA is given in Fig. 8 [79]. In earlier TEM work, no CSRO can be detected from these observations under the [110] zone axis, and the selected area nanobeam electron diffraction pattern (EDP) shows no additional diffraction information besides the normal FCC Bragg spots [86,87]. While a different situation is observed from the [112] zone axis (Fig. 8). Besides the expected FCC spots, highly diffuse extra disks, which are in the $\frac{1}{2}\{\bar{3}11\}$ positions (as indicated by the arrows in Fig. 8a), can also be observed. Much better contrast and clearer observation for these diffuse extra disks can be illustrated in the nanobeam EDP (Fig. 8b). These diffuse extra disks in reciprocal space with size several times that of the normal Bragg spot, definitely indicate the existence of additional ordering with a very small spatial extent in real space. Indeed, the size of most these CSRO regions is less than 1 nm and the area fraction of them is about 25 %, as revealed by the dark-field TEM image utilizing the extra reflections (Fig. 8c), and the average size is about 0.6 nm (Fig. 8d). Diffuse extra reflections can be observed again using the high-angular dark-field lattice image and the corresponding pattern of fast Fourier transformation (FFT) along the [112] zone axis (Fig. 8e). Superimposing the inverse FFT images for the CSRO regions (Fig. 8f) and normal FCC lattice (Fig. 8g) can result in an overlapped image (Fig. 8h), in which the CSRO regions can be more clearly observed. As indicated in the inset of Fig. 8h, the periodic lattice planes for planes in the FCC matrix, which is consistent with the results of the diffuse extra disks appearing at the locations of $\frac{1}{2}\{\bar{3}11\}$ positions. These observed CSROs with size below 1 nm are expected to have great influences on the mechanical properties of MEAs/HEAs, especially on strengthening and strain hardening by interactions with moving

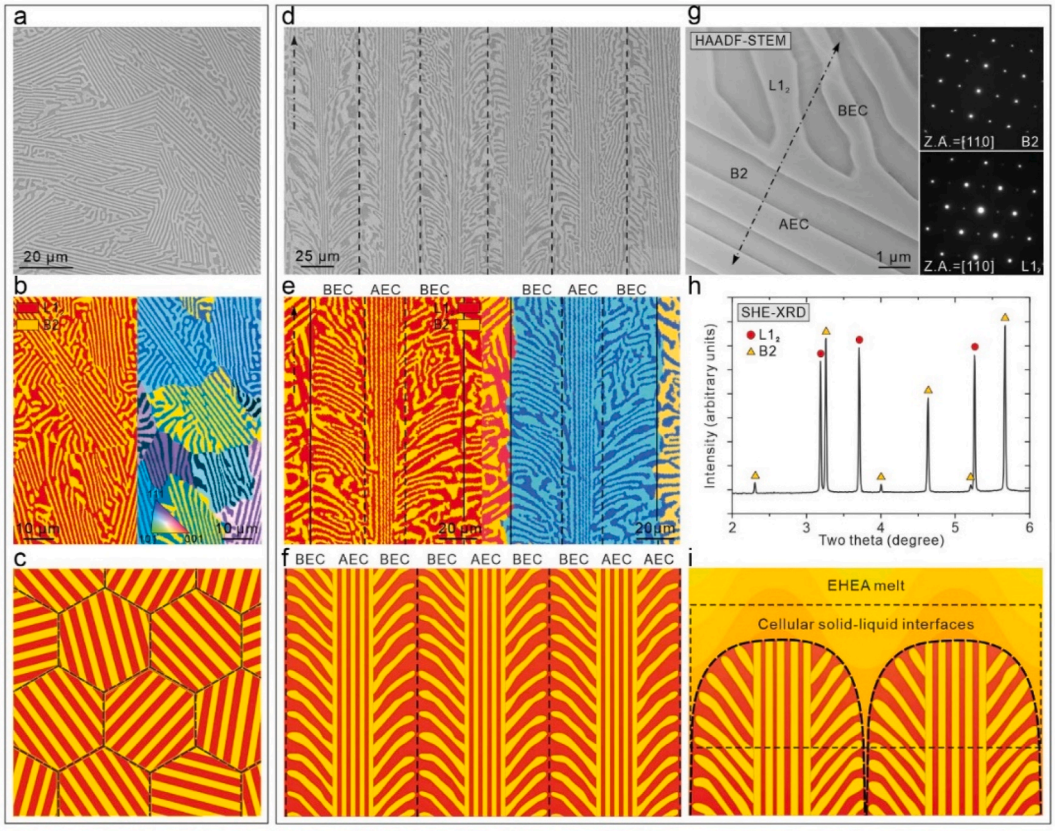

Fig. 7. A hierarchical eutectic structure in the $Al_{19}Fe_{20}Co_{20}Ni_{41}$ HEA. (a–c) Conventionally cast eutectic HEA. (d–i) The directionally solidified eutectic HEA with a hierarchical herringbone microstructure. Reproduced from Ref. [51].

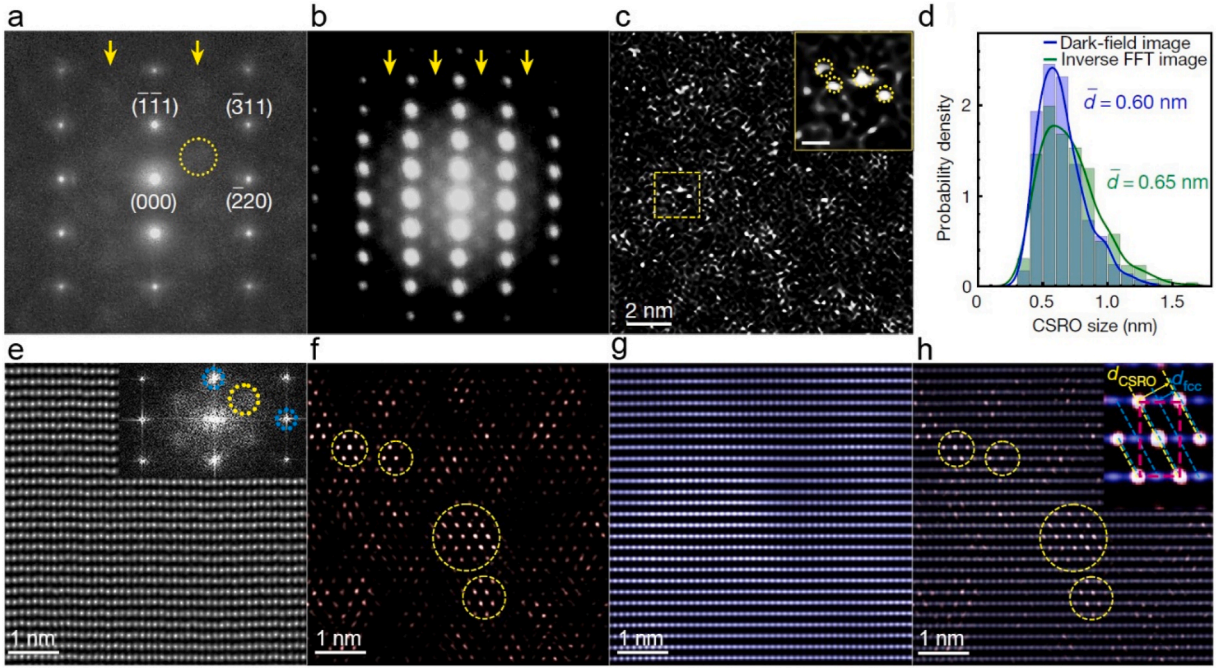

Fig. 8. The chemical short-range order in the VCoNi HEA. (a) Selected-area electron diffraction pattern (EDP). (b) Nano-beam EDP. (c) Energy-filtered dark-field TEM image. (d) The size distribution of the CSRO regions. (e) Lattice image of the fcc phase. (f–h) Inverse FFT image showing the CSRO regions, fcc lattice, and the superimposing. Reproduced from Ref. [79].

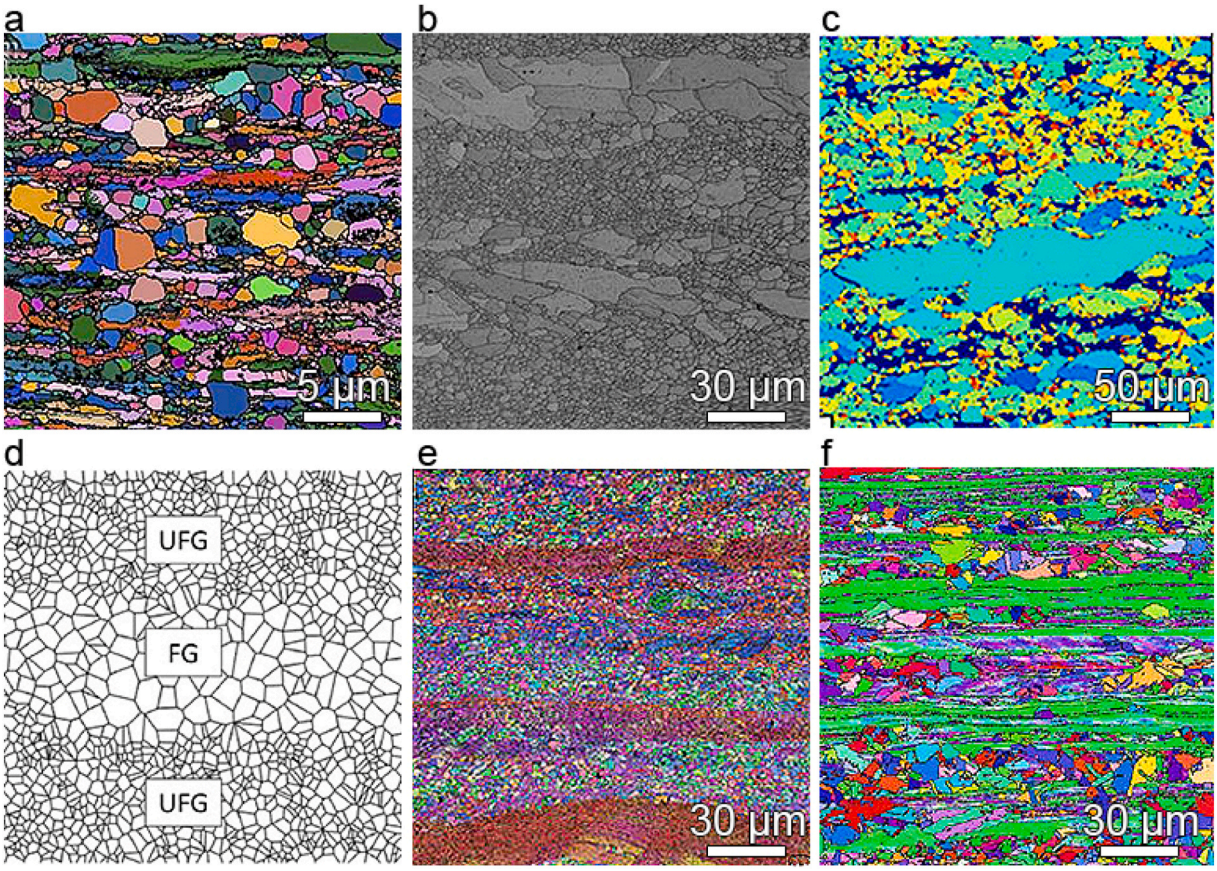

Fig. 9. The heterogeneous lamellar structures in (a) Ti alloy, (b–e) FeNiCoAlTaB HEA, and (f) FeCoNi. Reproduced from Refs. [43,89,90].

dislocations [79].

2.5. Heterogeneous lamella structures

Recently, the heterogeneous lamella (HL) structures have been reported to be a near-ideal heterostructured [43,88]. HL structure was originally obtained in commercial pure Ti processed by asymmetric rolling and subsequent partial recrystallization annealing [43]. In the HL structure, the recrystallized soft lamellae are embedded in the nano-recrystallized but recovered nanostructured matrix (Fig. 9a), which can produce hetero-deformation-induced (HDI) strengthening and HDI strain hardening effectively [43]. This design concept was also extended into MEAs/HEAs [89,90]. For example, Zhang et al. [88] designed a metastable FeNiCoAlTaB HEA with HL structure, showing the fine-grained bands combined with coarse-grained lamella over a large length scale. As shown in Fig. 9b and c, the ultrafine grains have an average size of 5 μm, and the coarse grains have an average size of 25 μm. The divergence of the grain size in this HL structure is caused by the different grain growth rates in the shear bands with high-angle boundaries and deformation bands and a few micro bands with low-angle boundaries, formed in the cold rolling process [89]. Upon annealing and aging, the nano-scale coherent γ' precipitates were formed in the fcc matrix, restricting the further grain growth of the initial recrystallized grinas by the Zener pining effect [88,91]. The initial deformation bands and heterogeneous precipitation result in the formation of the HL structure. By the same strategy, Ding et al. also designed the HL structures in an equiatomic ternary CoNiFe MEA, as shown in Fig. 9f [90].

3. Deformation and hardening of heterostructured materials

In the following part, we review the plastic deformation of diverse heterostructures in the tensile test. The corresponding microstructural mechanism of the plastic deformation and the HDI stress and strain hardening are discussed deliberately.

3.1. Gradient structure

The trade-off relationship between the strength and ductility in HEA also exists since there is no difference in plastic deformation features compared to conventional metals. However, Pan et al. [55]. reported that $Al_{0.1}$CoCrFeNi HEA with gradient structure exhibited exceptional strength and ductility. As shown in Fig. 10a, the single phase fcc $Al_{0.1}$CoCrFeNi HEA with gradient dislocation cell structure (GDS) showed an excellent combination of yield strength and ductility in ambitious temperature and liquid-nitrogen temperature [55,56]. The tensile yield stress of the GDS samples is up to 362–539 MPa, which is about 2~3 times as strong as the fine-grained (FG) and coarse-grained (CG) counterparts (~185 MPa). At the same time, the uniform elongation of the GDS samples was measured up to 43–48 %, which is slightly reduced relative to that of CG and FG counterparts. This means that the gradient cell-structured HEA seems to have the ability to overcome the long-standing strength-ductility trade-off. From a microscopic viewpoint, the trade-off relationship between strength and ductility is related to the strain-hardening capacity of the structures, since the strength and ductility are both governed by the motion of crystal defects [92,93]. As shown in Fig. 10b, the GDS samples showed a steady strain hardening with a lower reduction rate, from 1.28 GPa at 3%-strain to 0.99 GPa at the necking strain. From the TEM observations of the GDS sample at 40%-strain (Fig. 11), the GDS sample-level structural gradient induced the progressive formation of a high density of tiny stacking faults (SFs) and twins from core to surface, nucleating from those abundant low-angle dislocation cells compared to that from grain boundaries (GBs) in the uniform structure [94]. On the other hand, the gradient plastic deformation in the sample-level heterostructure motivated a complex stress-strain state with stress partition and back stress. Consequently, the SF-induced plasticity and resultant refined structures, coupled with back stress hardening and gradient plastic deformation, contribute to enhanced ductility, increased strength, and elevated strain hardening [95,96].

The nanostructured topmost layer always starts necking prematurely after yielding due to the intrinsic low strain hardening capability, so suppressing the early failure of the nanostructured layer is crucial for achieving better ductility in the gradient structure [97]. Qin et al. [36] designed a duplex gradient structure in the $Al_{0.5}Cr_{0.9}FeNi_{2.5}V_{0.2}$ HEA, combining the grain-size gradient with the gradient distributed $L1_2$ precipitate along the depth of the sample (Fig. 3). The yield strength and ductility of the duplex gradient structure (blue line in Fig. 12a) were improved simultaneously compared to the single gradient structure (black line in Fig. 12a). The duplex gradient structure showed a significantly higher strain hardening rate, as shown in Fig. 12b. The higher HDI stress and larger HDI strain hardening were obtained in the duplex gradient structure (Fig. 12c and d). According to microstructure observation, the higher density of GNDs was produced in the duplex gradient structure accompanied by the stronger precipitation hardening by the $L1_2$ and B2 precipitates [36].

3.2. Heterogeneous grain structures

Developing advanced HEA with high yield strength is a long-standing pursuit for the application of structural materials, especially for more than 1 GPa yield strength. Heterogeneous grain-structured HEAs showed a promising combination of higher yield strength and

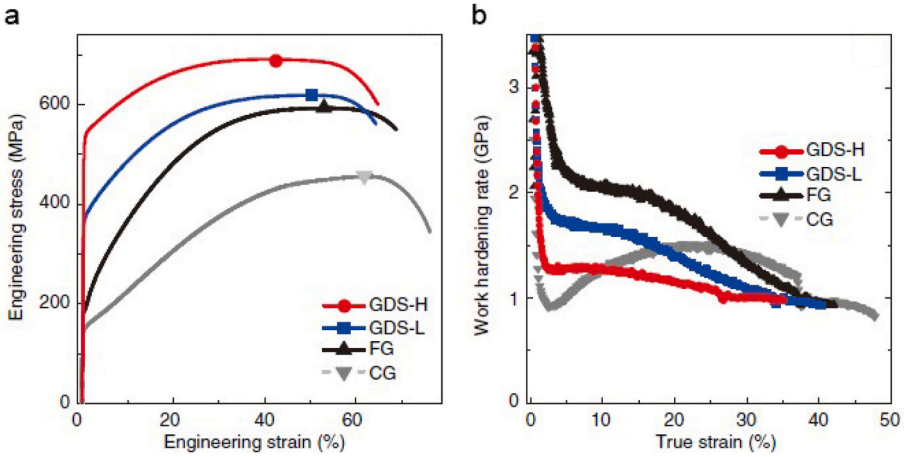

Fig. 10. Tensile stress-strain curves (a) and strain hardening rate (b) of GDS HEA. Reproduced from Ref. [55].

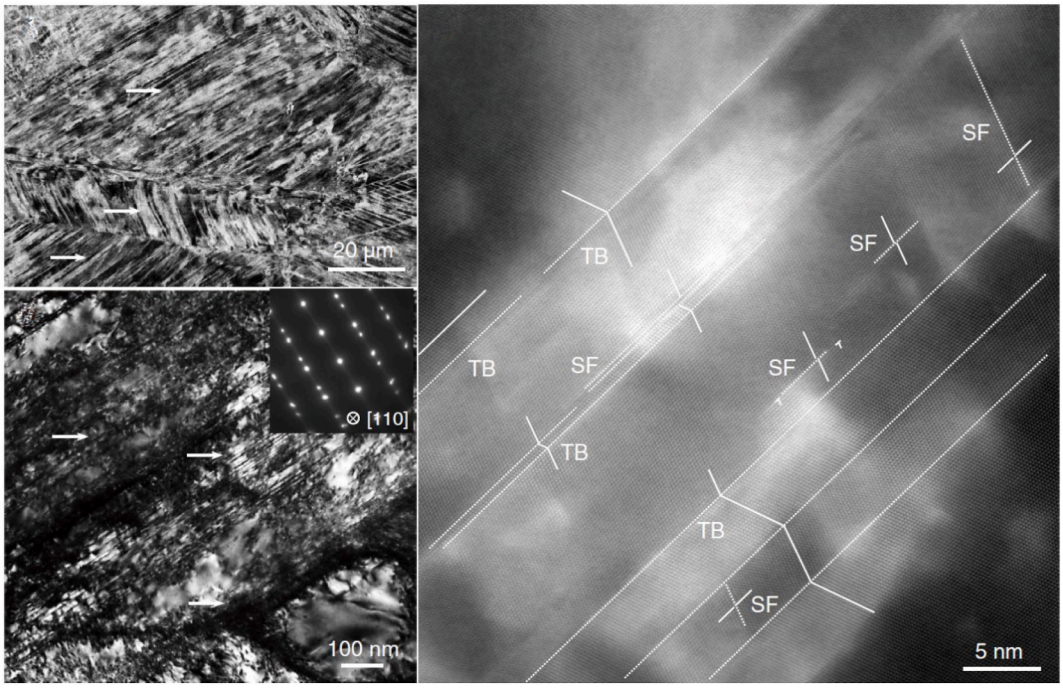

Fig. 11. Stacking faults of the GDS HEA at 40%-tensile strain. Reproduced from Ref. [55].

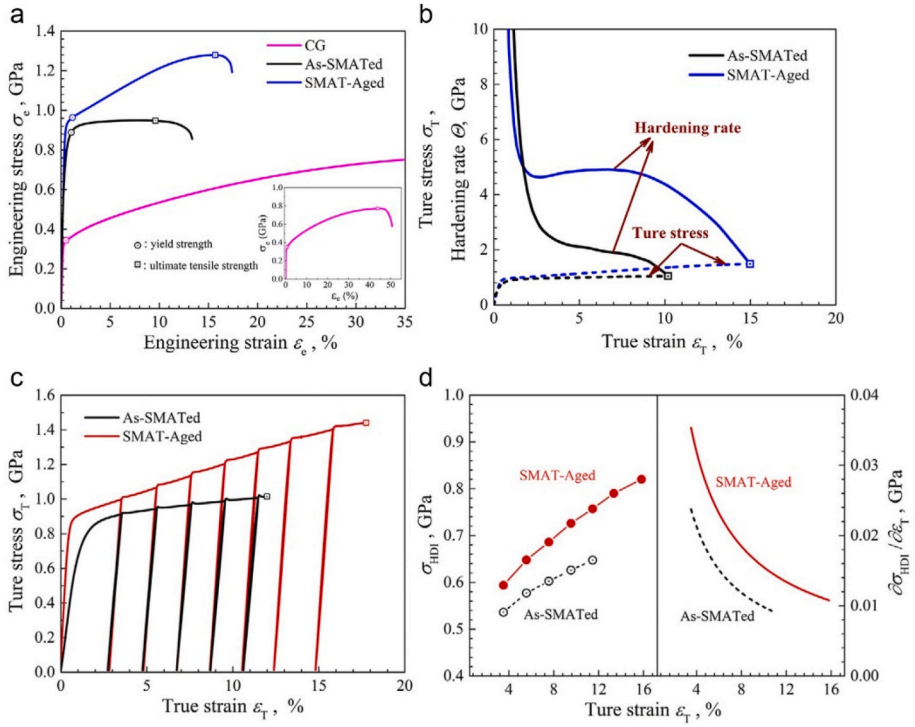

Fig. 12. Tensile properties and HDI hardening of the duplex gradient structured HEA. (a) Stress-strain curves. (b) Strain hardening rate curves. (c) True stress-strain curves of LUR test. (d) HDI stress and HDI hardening curves. Reproduced from Ref. [36].

sufficient ductility [22,39,67,98]. As shown in Fig. 13a, the yield strength of the heterogeneous structured $CoCrNiAl_3Ti_3$ MEA achieved up to 2.0 GPa, and the ultimate yield strength was up to 2.2 GPa with a uniform elongation of up to 13 % at ambient temperature [67]. The heterogeneous coherent L12 nanoprecipitates with a total of 24.2 % in volume fraction took more than half of the yield strength (~1115 MPa). At the same, the coherent precipitates minimize the elastic misfit strain of interfaces resulting in alleviating the stress concentration and enhancing ductility [99,100]. The single-phase CoCrNi MEA with a three-level heterogeneous grain structure (HGS) exhibited a yield strength of 1.2 GPa and a uniform elongation of 22 % at room temperature (red line in Fig. 13b), and simultaneously increase to 1.5 GPa and 36 % respectively, at 77 K (blue line in Fig. 13b). As the result showed, the HGS imparts load partitioning to promote back stress hardening (later called HDI hardening), which is further aided by dynamically generated twinned nano grains at the grain corners and grain boundaries

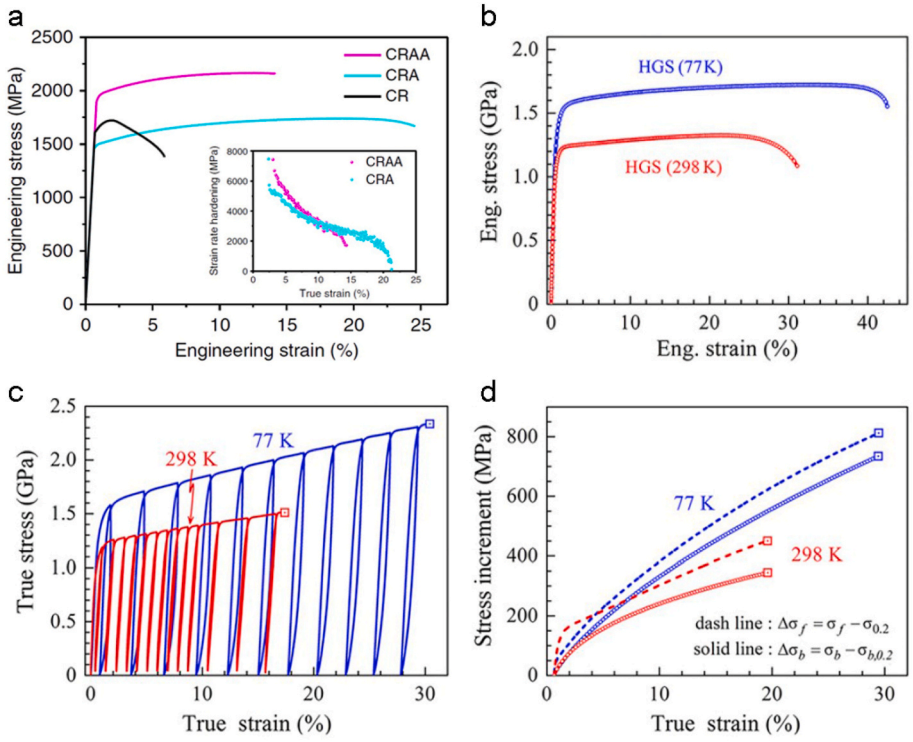

Fig. 13. Tensile stress-strain curves of (a) HGS $CoCrNiAl_3Ti_3$ MEA and (b) HGS CoCrNi MEA. (c–d) Load-unload-reload tensile curves and back stress of HGS CoCrNi MEA. Reproduced from Refs. [39,67].

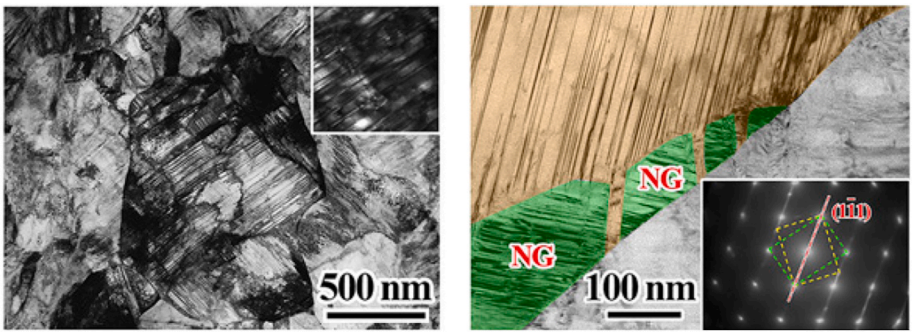

Fig. 14. Dynamic generation of nanograins at GBs during tensile straining in HGS CoCrNi MEA. Reproduced from Ref. [39].

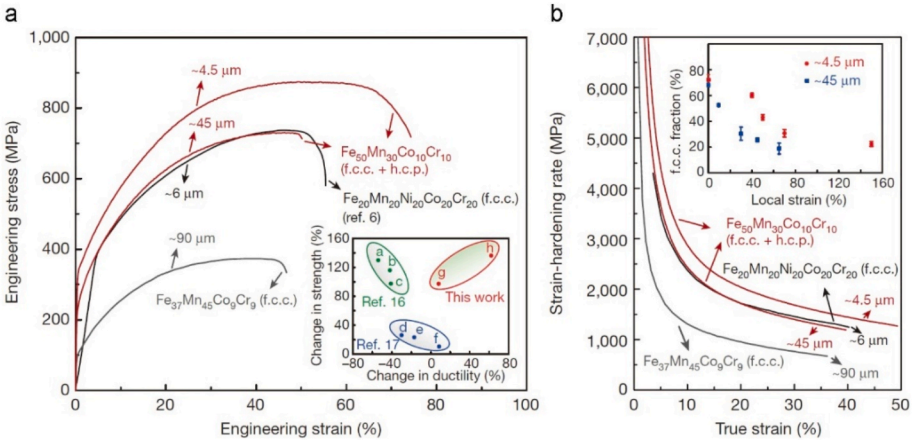

Fig. 15. Tensile stress-strain curves (a) and strain hardening rates (b) of the TRIP-DP-HEAs compared to various sing-phase HEAs. Reproduced from Ref. [50].

(Fig. 14). This dynamic grain refinement during tensile strain resulted in a record-wide hysteresis loop in the load-unload-reload curve and high back stress hardening, in the absence of any second phase (Fig. 13c and d). This report shows a processing route for the single-phase alloys with low stacking fault energy (SFE) to achieve a larger ductility at the high yield strength.

3.3. Dual-phase or multiple-phase structures

As discussed earlier, the stacking faults and deformation twinning companying with the dislocation interaction are prevalent in the deformation of single-phase HEAs [29,94]. While in dual-phase or multiple-phase HEA, the deformation-driven transformation was realized well through metastable engineering for providing additional strain hardening [50]. As shown in Fig. 15a, the metastable dual-phase $Fe_{50}Mn_{30}Co_{10}Cr_{10}$ HEA exhibited lower yield strength of about 200–300 MPa, but vastly higher tensile ultimate strength and ductility, those are 700~850 MPa and 45 %–60 %, respectively, as well as the enhanced strain hardening rates [50]. As revealed by EBSD phase maps (Fig. 16), the fcc phase transforming to the hcp phase was the primary deformation mechanism. Furthermore, the volume fraction of the phase transformation for grain-refined HEA is the same as that of coarse-grained HEA, while the ductility was extended (inset of Fig. 15b). These results revealed phase transformation plays an important role in plastic accommodation and hardening, and optimizing the phase stability could also increase ductility to some extent [50].

Except for the TRIP HEA, another type of dual-phase HEA is the eutectic HEA. Shi et al. [72] architected a dual-phase $AlCoCrFeNi_{2.1}$ HEA with a heterogeneous lamella structure. As shown in Fig. 17a, the dual-phase heterogeneous lamella (DPHL) HEA exhibited a simultaneous strength-ductility enhancement compared to the ultrafine-grained counterpart and the as-cast sample. The three-condition DPHL HEA (the numbers are annealing temperatures in Fig. 17b) both have a yield strength of more than 1.1 GPa along with ductility of larger than 14 %, which is not accessible to the previously reported methodologies [72]. Even the phase transformation did not work in this dual-phase HEA, the self-generated microcracks were conducted along the phase boundaries, as shown in Fig. 17c and d. These microcracks could buffer the local strain concentration and delay the catastrophic failure [51,72].

3.4. Heterostructure lamella structures

The heterostructure lamella structured (HL) FeNiCoAlTaB (referred to here as NCATB, black line in Fig. 18a) HEA achieved a better combination of strength and ductility compared to the fine-grained sample (purple line in Fig. 18a), resulting from the higher strain hardening capability (shown in Fig. 18b) [89]. The HL NCATB HEA combining the γ' precipitates showed an exceptional combination of strength and ductility [88]. As shown in Fig. 18c, the NCATB-0, NCATB-2, and NCATB-5 represented the HL HEA aging for 0 h, 2 h, and 5 h [88]. The HL HEA after aging exhibited a significant enhancement in yield strength and ductility, showing yield strength of 1.1 GPa and 1.4 GPa, and ultimate tensile strength of 1.4 GPa and 1.7 GPa with total elongation of 30 % and 10 %, for NCATB-2 and NCATB-5, respectively. As compared to the heterostructure metals, some TRIP/dual phase/maraging steels, and homogeneous HEAs, the HL HEA with precipitation hardening showed much better tensile properties, although these groups all suffer from the classic strength-ductility trade-off [88].

4. Fracture and fatigue behavior of heterostructured materials

Fracture behaviors of materials are fundamental issues and provide a great challenge in the applications of both engineering structural and non-structural components. Historically, significant losses and costs has been incurred due to unforeseen fracture events [101]. Therefore, the development of both strong and tough (damage-tolerant) materials is imperative for diverse applications in industries [102,103].

The fracture behaviors of materials are highly dependent on microstructure, stress state, temperature, and loading rate. These fracture behaviors can be broadly classified into brittle or ductile modes [104]. Prior to their engineering applications, extensive investigations of fracture resistance for all materials are generally required. The term "fracture toughness" is commonly employed to refer to the material resistance against crack initiation and extension, typically determined at the critical point where unstable cracking initiates [105–108]. Three fundamental fracture modes and their combinations can be identified in engineering applications, while the mode I fracture is the most frequent failure mode in practical applications [109]. Under small-scale yielding conditions in plane strain, the critical value of the linear elastic stress intensity factor (K_{IC}) can be determined by measuring the onset of crack initiation [101,108]. Moreover, the critical value of the J-integral (J_{IC}) can effectively characterize the fracture toughness in the elastic-plastic material [110–112]. Two parameters are interrelated under the condition of small-scale yielding: $J_{IC} = \frac{K_{Ic}^2}{E'}$, $E' = E$ in plane stress or $E' = E/(1\text{-}\upsilon^2)$ in plane strain, where E is the elastic modulus and υ is Poisson ratio.

The strength and fracture behavior can be analyzed in terms of intrinsic (plasticity) and extrinsic (shielding) toughening mechanisms associated with the crack extension [103,113], as shown in Fig. 19. The illustration depicts the competition between intrinsic toughening mechanisms, which operate ahead of the crack tip to enhance fracture resistance, and extrinsic toughening mechanisms, which are active at or behind the crack tip. Intrinsic toughening is primarily driven by plastic deformation. However, extrinsic toughening can decrease the local stress and strain fields near the crack tip through processes such as crack deflection and crack bridging.

In recent years, numerous studies have been undertaken to characterize the fracture resistance of diverse MEA/HEA systems, significantly advancing our comprehensive understanding of their mechanical properties and the underlying mechanisms that lead to failure

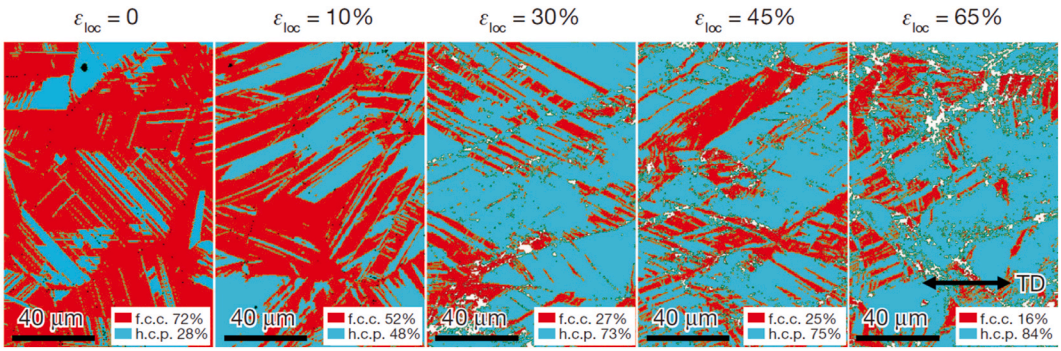

Fig. 16. EBSD phase map revealing the martensitic transformation of TRIP-DP-HEA. Reproduced from Ref. [50].

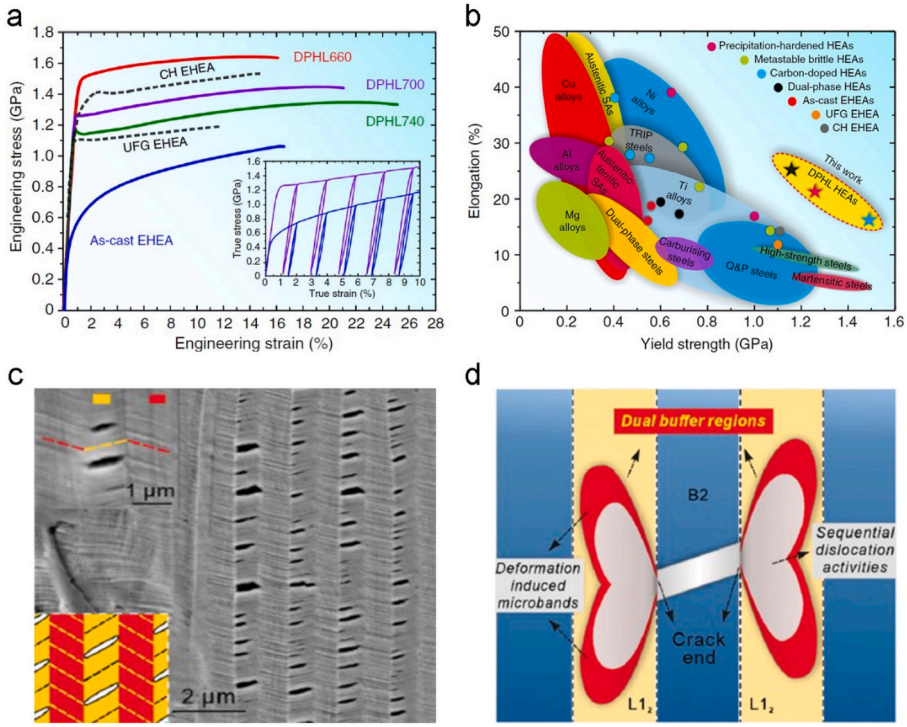

Fig. 17. Tensile properties, self-generated microcracks, and buffering mechanism of the DPHL HEA. (a) Engineering stress-strain curves. (b) Tensile properties. (c) Hierarchical crack buffering. (d) Schematic diagram of crack buffering. Reproduced from Refs. [51,72].

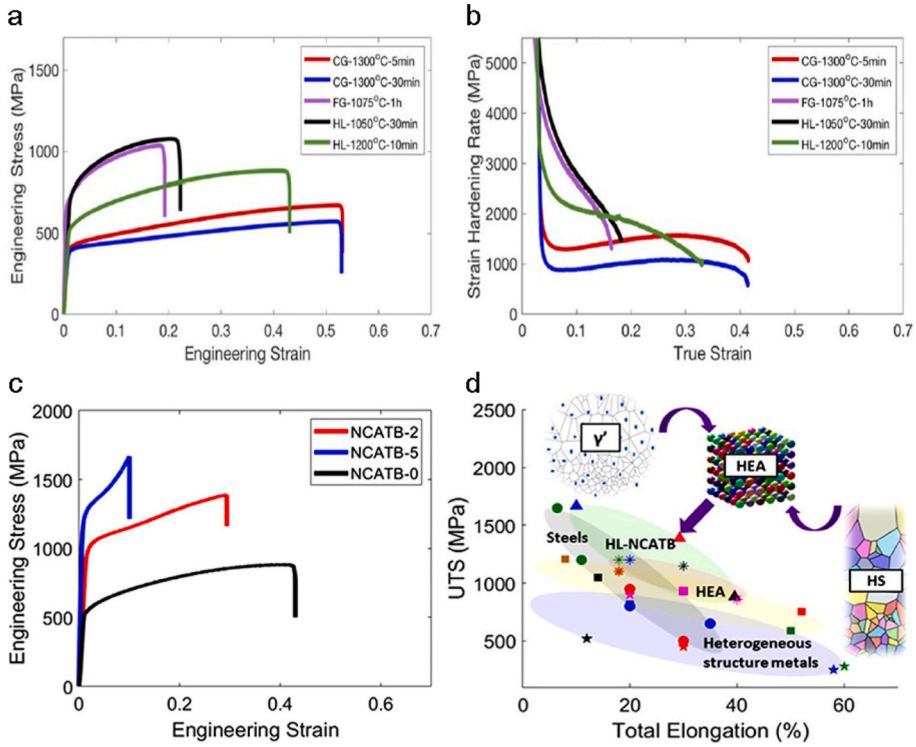

Fig. 18. (a–b) Tensile stress-strain curves and strain hardening rate of HL FeNiCoAlTaB HEA. (c–d) Tensile response and mechanical properties of HL FeNiCoAlTaB HEA with precipitates. Reproduced from Refs. [88,89].

[114–119]. The MEA/HEAs composed primarily of a single FCC phase generally exhibit high fracture toughness, whereas BCC MEA/HEAs demonstrate significantly low values. On the other hand, those with a dual-phase structure tend to show intermediate fracture toughness values. In this section, the recent advancements in characterizing the fracture behaviors of MEA/HEAs with heterogeneous structures are succinctly outlined, aiming to offer valuable insights and guidance for future research endeavors.

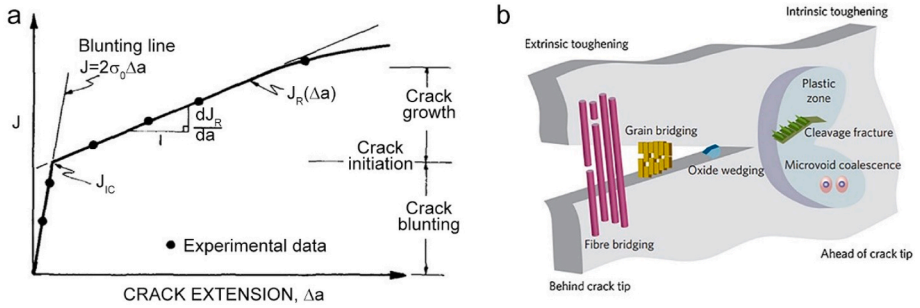

Fig. 19. (a) $J_R(\Delta a)$ crack-resistance curve (R-curve) describing the position of the J_{Ic} at the initiation of crack growth where the resistance curve intersects with the blunting line. Reproduced from Ref. [108]. (b) Schematic drawing describing the intrinsic and extrinsic toughening mechanisms in terms of the crack advance. Reproduced from Ref. [103].

4.1. Heterogeneous grain/lamella structures

Gludovatz and Liu et al. [94,116,120] have conducted extensive research on the damage tolerance of CrCoNi and CrMnFeCoNi MEA/-HEAs, which feature a single-phase FCC solid solution and heterogeneous grain structures. These alloys exhibit remarkable strengths and damage tolerances, achieving tensile strength exceeding 1 GPa and fracture toughness value surpassing 200 MPam$^{1/2}$. Furthermore, their mechanical properties actually become better as the temperature decreases, especially in the case of ultra-low temperature (~20 K). The plot in Fig. 20 illustrates the fracture toughness values of CrCoNi and CrMnFeCoNi MEA/HEA with heterogeneous structures as a function of varying temperatures.

The planar-slip dislocation activity is the primary deformation mode at room temperature, especially for the CrMnFeCoNi HEA. The SEM images for fracture surfaces indicate the ductile fracture mode of the CrMnFeCoNi by the coalescence of microvoids, with a more distorted crack path at the lower temperature. However, as the temperature decreases, nano-twinning emerges as a crucial additional source of strain hardening, indicating that the earlier initiation of deformation nano-twinning holds the key to achieving exceptional damage tolerance. Furthermore, the concurrent activation of multiple strain-hardening mechanisms, including stacking faults, fine nanotwins, and transformed ε-martensite, at approximately 20 K, as depicted in Fig. 21, can effectively facilitate the arrest and the transmission of dislocations, thus further enhancing the strength and ductility.

While FCC-structured MEA/HEAs with coarse grains can exhibit excellent mechanical properties, a typical increase in yield strength achieved through grain refinement often comes with a compromise in toughness, creating a balance between strength and toughness, particularly at gigapascal levels. Liu et al. [121] reported that an N-doped CrCoNi MEA exhibited exceptional fracture toughness and a yield strength exceeding 1 GPa, attributed to its heterogeneous structural characteristics. In the heterogeneous lamella structure, the fracture toughness reaches 91 MPa·m$^{1/2}$ at a yield strength of 1.3 GPa, while in the heterogeneous grain structure, it attains 168 MPa·m$^{1/2}$ at a yield strength of 1.0 GPa. The superior fracture toughness can be attributed to the forest hardening and an extra HDI hardening. The pile-ups of GNDs are observed to be formed at the domain boundaries to accommodate strain gradient at the plastic zone of the crack tip. Additionally, the presence of CSRO regions has been observed to enhance strain hardening near the crack tip through its interaction with dislocations.

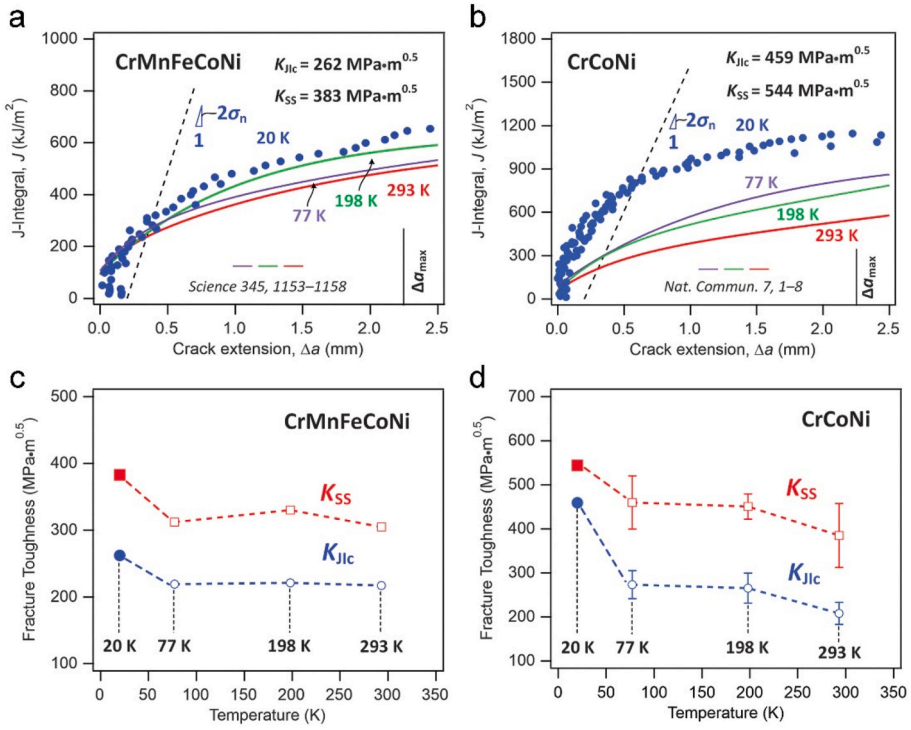

Fig. 20. Fracture toughness of heterogeneous CrMnFeCoNi (a, c) and CrCoNi (b, d). Reproduced from Ref. [120].

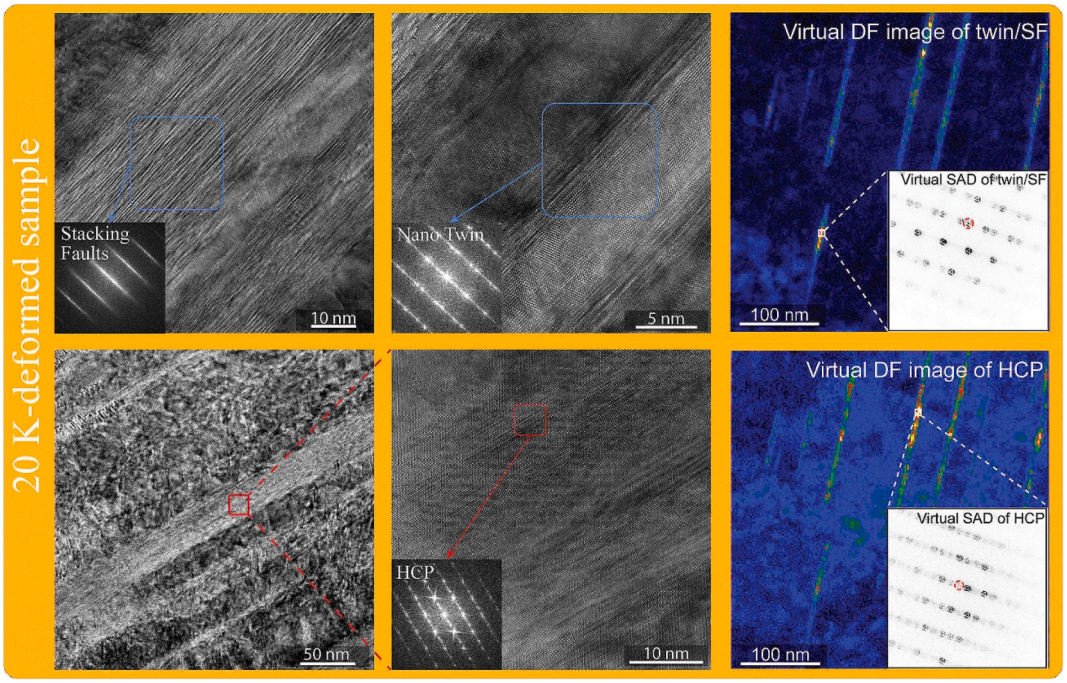

Fig. 21. Deformed microstructures in the heterogeneous structured CoCrNi MEA. Reproduced from Ref. [120].

4.2. *Dual-phase structures*

The development of dual-phase eutectic HEAs (EHEAs) [122–125] presents an alternative methodology for significantly enhancing their mechanical properties, encompassing hardness, strength, plasticity, and toughness. A series of heterostructured EHEAs, such as $CoCrFeNiNb_{0.5}$ (FCC + Laves), $Al_{(18-2x)}Co_{30}Cr_{(11+x)}Fe_{(11+x)}Ni_{30}$ (FCC + Sigma) and $CoCrNiMo_x$ (FCC + BCC), have been designed to study the synergy of fracture toughness and strength/hardness by adjusting the fraction of constituent phases [126–128]. As the FCC content decreases, the fracture toughness diminishes while the strength escalates. Fig. 22 showcases an Ashby plot that depicts the correlation between fracture toughness and yield strength across various single-phase and dual-phase MEA/HEAs.

The investigation of metastable dual-phase (DP) HEAs has also been conducted. The yield strength and fracture toughness of the $Fe_{50}Mn_{30}Co_{10}Cr_{10}$ (DP-HEA), consisting of FCC and HCP phases, are determined to be approximately 266 MPa and 205 MPa·m$^{1/2}$, respectively, which are comparable to that of CrMnFeCoNi [129]. The addition of C as an alloying element into DP-HEA ($Fe_{49.5}Mn_{30}Co_{10}Cr_{10}C_{0.5}$, C-DP-HEA) results in a 47 % increase in fracture toughness (K_{IC} = 301 MPa·m$^{1/2}$) compared to the DP-HEA without the addition of C [130]. The addition of C into DP-HEA leads to an elevation of the stacking fault energy, thereby enhancing the stability of the FCC phase [131]. Thus, in C-DP-HEA, the primary deformation mechanism is strain-induced martensitic transformation, with nano-twinning also playing a significant role in the deformation process. The enhanced strain hardening observed in C-DP-HEA can be attributed to the presence of additional obstacles, arising from the increased density of twin boundaries and phase boundaries. The strain hardening enhances fracture toughness by facilitating plastic deformation ahead of the crack tip, thereby retarding the crack initiation and propagation. The $Si_xV_{(9-x)}Cr_{10}Mn_5Fe_{46}Co_{30}$ FCC-based metastable HEAs were also developed by precisely manipulating the relative phase stabilities based on equilibrium phase diagrams and Gibbs free energies [132,133]. The stability of FCC decreased with increasing Si content, leading to a transformation from FCC to HCP. Meanwhile, the cryogenic fracture toughness often diminishes due to a diminished damage tolerance capacity, resulting from the occurrence of a ductile-brittle transition phenomenon when a significant amount of BCC martensite undergoes transformed [134,135]. An exceptional combination of strength and ductility achieved, particularly at 77K, can be attributed to the remarkable strain-hardening effect resulting from the FCC-HCP-BCC deformation-induced martensitic transformation, as illustrated in Fig. 23. The $Si_8V_2Fe_{45}Cr_{10}Mn_5Co_{30}$ exhibits a significantly high fracture toughness (K_{IC} = 292 MPa·m$^{1/2}$) and a ductile-dimpled fracture mode at room temperature. At 77K, however, the fracture toughness was significantly reduced, and the brittle fracture of lamellar cleavage facets was characterized by the ladder-shaped arrangement of plate-type BCC martensite, which exhibited a lower number of phase boundaries and GNDs.

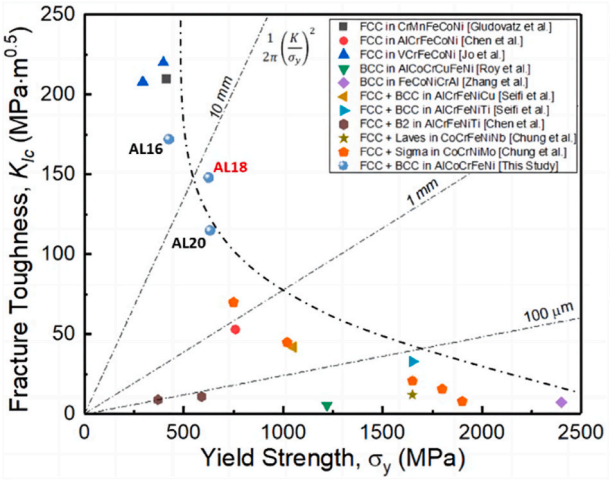

Fig. 22. Ashby plot of fracture toughness vs. yield strength for various MEA/HEAs. Reproduced from Ref. [126].

The nano-bridged honeycomb structured HEA consisting of FCC matrix and an interwoven hexagonal net of B2 phase exhibits an excellent combination of strength (~1 GPa) and toughness (~300 MPa·m$^{1/2}$) at both room and cryogenic temperatures [136]. The alloy is strengthened by impeding the mobility of dislocations at the early stage

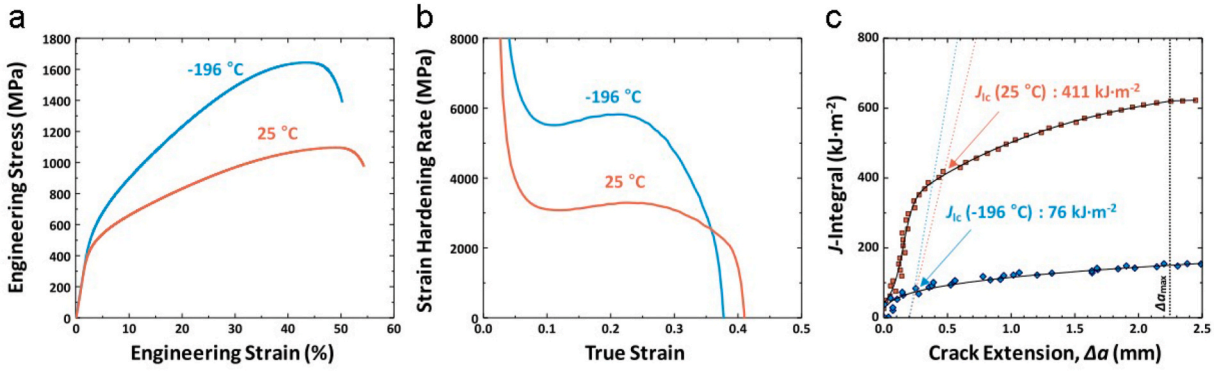

Fig. 23. (a) Engineering stress-strain curves, (b) strain-hardening-rate curves, and (c) crack-growth-resistance (J_R) curves of the $Si_8V_2Fe_{45}Cr_{10}Mn_5Co_{30}$ alloy tested at 25 and −196 °C. Reproduced from Ref. [132].

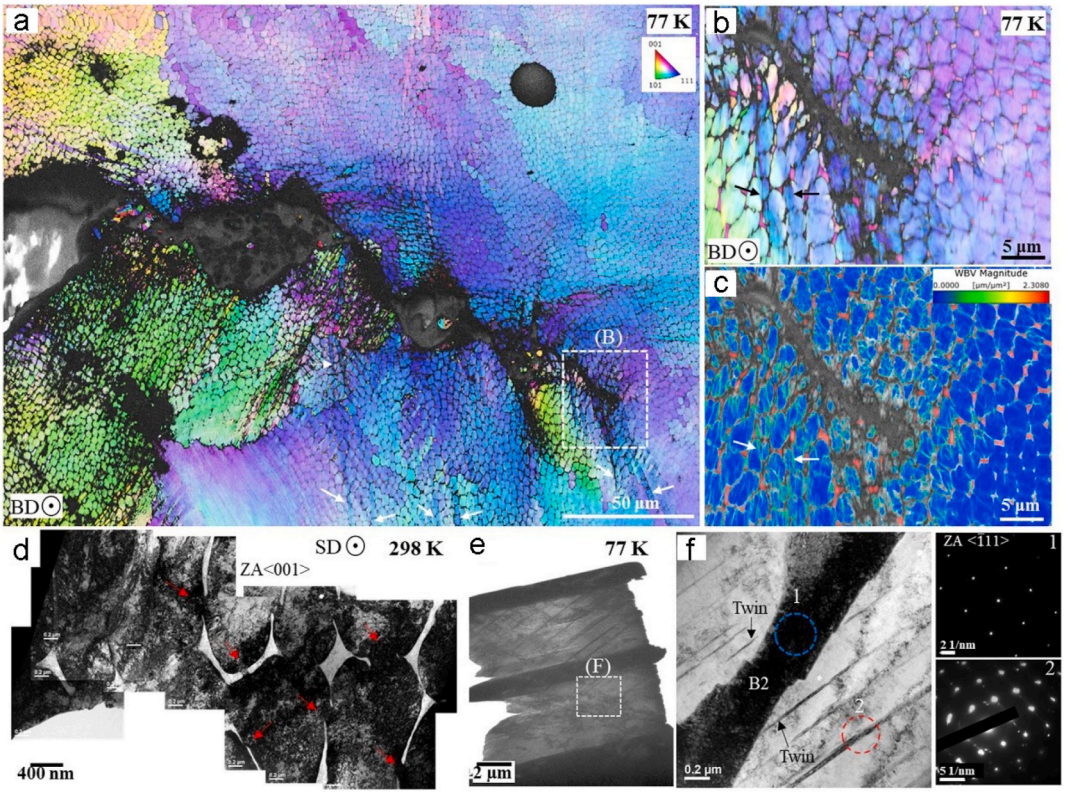

Fig. 24. Deformation mechanism in nano-bridged honeycomb structure HEA ($Al_{0.5}CrCoFeNi$) at 298 K and 77 K. (a–c) EBSD map showing the misorientation spreading away from the crack. TEM image near the crack-tip region of the specimen tested at 298 K (d) and 77 K (e–f). Reproduced from Ref. [136].

of plastic deformation. However, the dislocation movement is facilitated by the breaking down of the dislocation nano-bridge connecting the B2 phase near the crack tip, thereby improving the fracture resistance through blunting and shielding of the crack tip, as shown in Fig. 24.

In engineering applications, materials and structural components are frequently subjected to cyclic loading, a process that often leads to substantial damage and, ultimately, catastrophic failure [137–140]. Fatigue damage frequently lead to significant accidents due to its lack of visible deformation, and fatigue failure remains a primary cause of mechanical part failures, accounting for over 80 % of such incidents [141,142]. To mitigate this risk, it is advisable to employ materials with superior fatigue strength for the fabrication of structural components, subjected to cyclic loads, such as gears, blades, shafts, bearings, and springs [143,144]. Given the immense potential of MEA/HEAs as structural materials, the exploration of their long-life fatigue behaviors and failure mechanisms remains a promising area for further investigation [145]. This section offers a comprehensive overview of recent research endeavors delving into the fatigue behavior of MEA/-HEAs with heterogeneous structures.

The introduction of intermetallic precipitates is a commonly employed approach to enhance fatigue endurance, as it effectively improves fatigue strength [146]. Feng et al. [147] reported an $Al_{0.5}CoCr-FeNi$ HEA with improved fatigue life through the incorporation of ductile-transformable multicomponent B2 precipitates. The presence of multiple cyclic deformation mechanisms, such as dislocation slips, precipitation strengthening, deformation twinning, and reversible martensitic phase transformation, has been observed. The enhanced fatigue performance at low strain amplitudes, namely the high resistance to fatigue crack initiation, can be attributed to the exceptional elasticity, plastic deformability, and martensitic transformation of the B2-strengthening phase. Meanwhile, maintaining comparable fatigue life at high strain amplitudes, as shown in Fig. 25. The presence of the

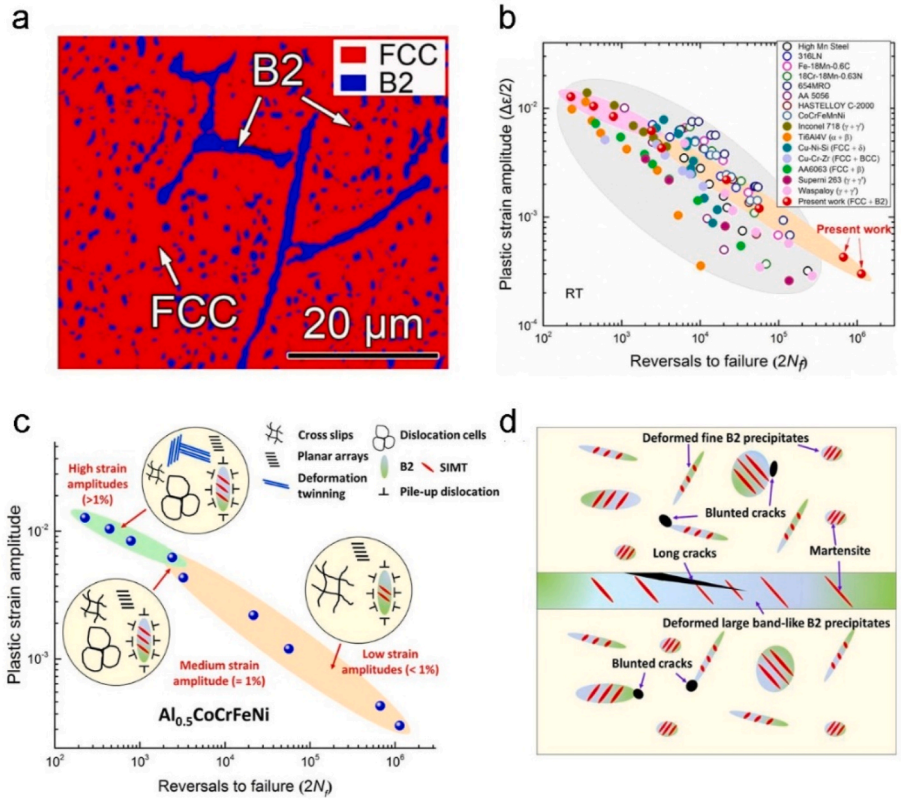

Fig. 25. Fatigue properties and microstructure mechanism of Al0.5 CoCrFeNi dual-phase HEA. (a) EBSD phase map. (b) Coffin-Manson fatigue data. (c) Summary of dominated cyclic-deformation mechanisms. (d) Schematic of the microcrack-formation mechanism during cyclic loading. Reproduced from Ref. [147].

fine ductile-transformable B2 phase effectively impedes the initiation of microcracks by harnessing stress relaxation and strain partitioning mechanisms during plastic deformation and martensitic transformation. This alleviates the cyclic accumulation of damage stemming from the deformation incompatibility between the B2 and FCC phases [148]. The ductile-transformable nature of the multicomponent B2 phase arises from its lower antiphase boundary energy and pronounced local lattice distortions, facilitating easy transformation to an orthorhombic structure. However, the likelihood of microcrack initiation increases when the size of the B2 phase, particularly in band-like formations, surpasses a specific threshold due to the presence of elongated incoherent interfaces. The multicomponent B2 phase could not only strengthen the soft FCC matrix but also coordinate the overall plastic deformation during monotonic and cyclic loadings. Furthermore, the occurrence of deformation twinning can also be induced during cyclic loading in a precipitation-strengthened HEA, which is typically challenging to observe under monotonic deformation at room temperature. This phenomenon provides an additional strengthening mechanism for enhancing fatigue life. Fig. 25c and d illustrates the schematics of the cyclic deformation mechanisms and the behavior of microcracks initiation observed in the dual-phase HEA.

4.3. Harmonic structures

The low cycle fatigue behavior and fatigue crack growth behavior of harmonic structured CoCrFeMnNi HEAs have been investigated in various research studies [149–151]. The fatigue behaviors are significantly governed by microstructure [152], thus prompting an investigation into the effect of shell fraction on low cycle fatigue and fatigue crack growth behaviors. Due to the enhanced strain hardening, the harmonic structured HEAs with a shell fraction ranging from 20 % to 40 % exhibit an exceptional combination of high strength, superior ductility, and excellent resistance to low cycle fatigue and fatigue crack growth. During the low-cycle fatigue process, the predominant occurrence of local plastic deformation is observed in the relatively softer core regions, which facilitates dislocation generation and rearrangement. This leads to an initial phase of cyclic hardening, followed by subsequent cyclic softening. The fatigue cracks propagate through both the core region (CG structure) and shell region (UFG structure) in harmonic structured samples. The propagation of cracks is hindered by the core region, resulting in the deflection of the cracks at the interface between the core and shell, as shown in Fig. 26. This phenomenon enhances the roughness of the fracture surface. The topology of the network core-shell grain structure is advantageous in augmenting the crack closure effect induced by surface roughness.

5. Dynamic behavior of heterostructured materials

The high strain rate response of materials plays a crucial role in engineering applications, such as vehicle crashworthiness, spacecraft protection and armor protection [153,154]. The deformation and fracture behaviors of metallic materials under impact conditions exhibit distinct performances compared to those observed under quasi-static conditions, owing to thermal softening effect, strain rate effect and inertia effect [155,156]. The thermal softening induced by adiabatic heating can facilitate strain localization, such as the formation of adiabatic shear band (ASB) [157,158]. The mechanisms underlying the mechanical properties have been extensively investigated for a century, leading to the development of a well-established plasticity theory based on three primary mechanisms: dislocation, TWIP, and TRIP. In rare cases of extreme deformation, an additional fourth mechanism involving the crystalline-to-amorphous transformation can also occur [159,160]. The present section succinctly summarizes the recent advancements in comprehending the dynamic response of MEA/HEAs with heterogeneous structures, aiming to offer valuable guidance for future research endeavors.

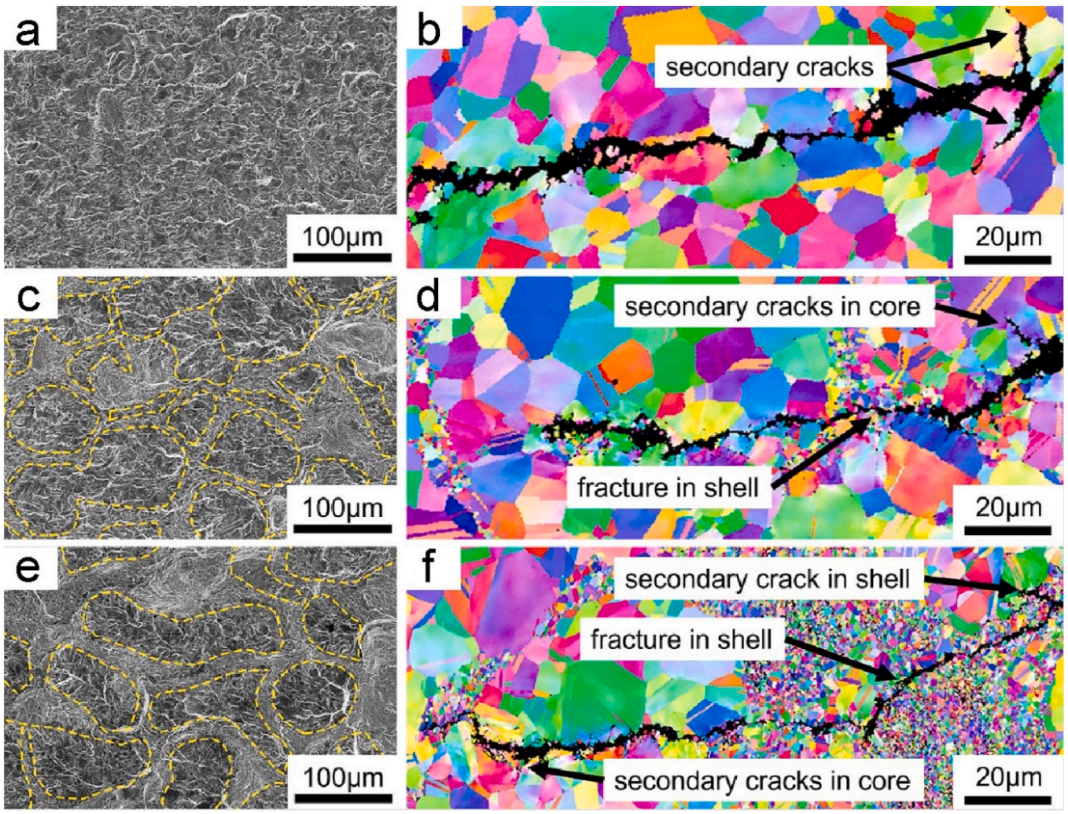

Fig. 26. Crack-path and fractography of sintered CoCrFeMnNi HEAs. (a,b) Shell area fraction is 0 %. (c,d) Shell area fraction is 23.6 %. (e,f) Shell area fraction is 42.6 %. Reproduced from Ref. [149].

5.1. Gradient structures

Qin et al. [161] designed a single gradient and dual gradient NiFe-$Cr_{0.9}Al_{0.5}V_{0.2}$ MEA for the dynamic shear tests using hat-shaped specimens in previous work. Here single gradient MEA represents only grain gradient distributed from the surface to the center by (surface mechanical attrition treatment) SMAT process on the CG samples. While dual gradient represents a combined grain gradient and a decreasing volume fraction of nanoprecipitates from the surface to the center by aging after the SMAT process (Fig. 3). The dual gradient MEA (solid pink line in Fig. 27) exhibited a synergetic strengthening and toughening effect as compared to the sole effect of the single gradient (dashed pink line in Fig. 27). The microstructure results showed that the higher magnitude of strain gradient and higher density of GNDs can be induced by the dual gradient structure, resulting in extra strain hardening [ZX-1]. Particularly, the ASB was delayed in initiating and propagating with about one magnitude lower velocity than in the homogeneous structured materials (Fig. 28) [161–163].

5.2. Heterogeneous grain structures

To improve the dynamic properties, we also introduced the heterogeneous grain structure in CoCrNi MEA through a combination of cold rolling and subsequent annealing at proper temperatures [40]. The HGS MEA exhibited outstanding dynamic shear properties, especially at cryogenic temperature (Fig. 29). The better performance of HGS MEA at cryogenic temperature was due to the more efficient grain refinement than at room temperature, resulting in stronger strain hardening capacity (Fig. 30). The deformation twins, stacking faults, Lomer-Cottrell locks, and phase transformation together are responsible for these outstanding dynamic shear properties [40,164].

HEAs with heterogeneous grain structures have demonstrated

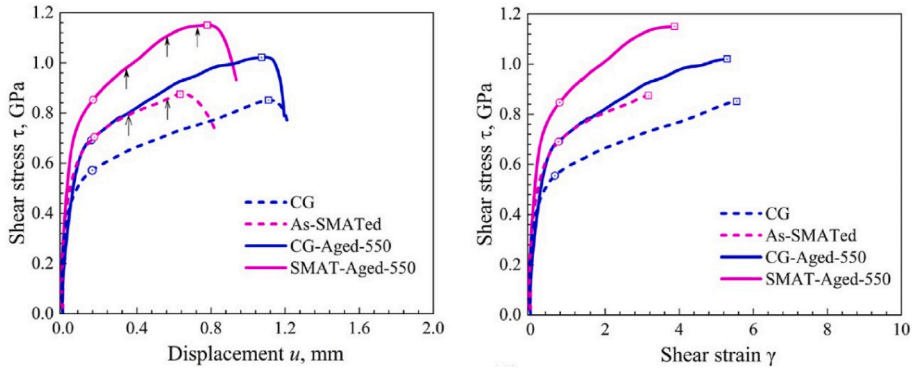

Fig. 27. Dynamic shear stress-displacement and strain curves of gradient $NiFeCr_{0.9}Al_{0.5}V_{0.2}$ MEA. Reproduced from Ref. [161].

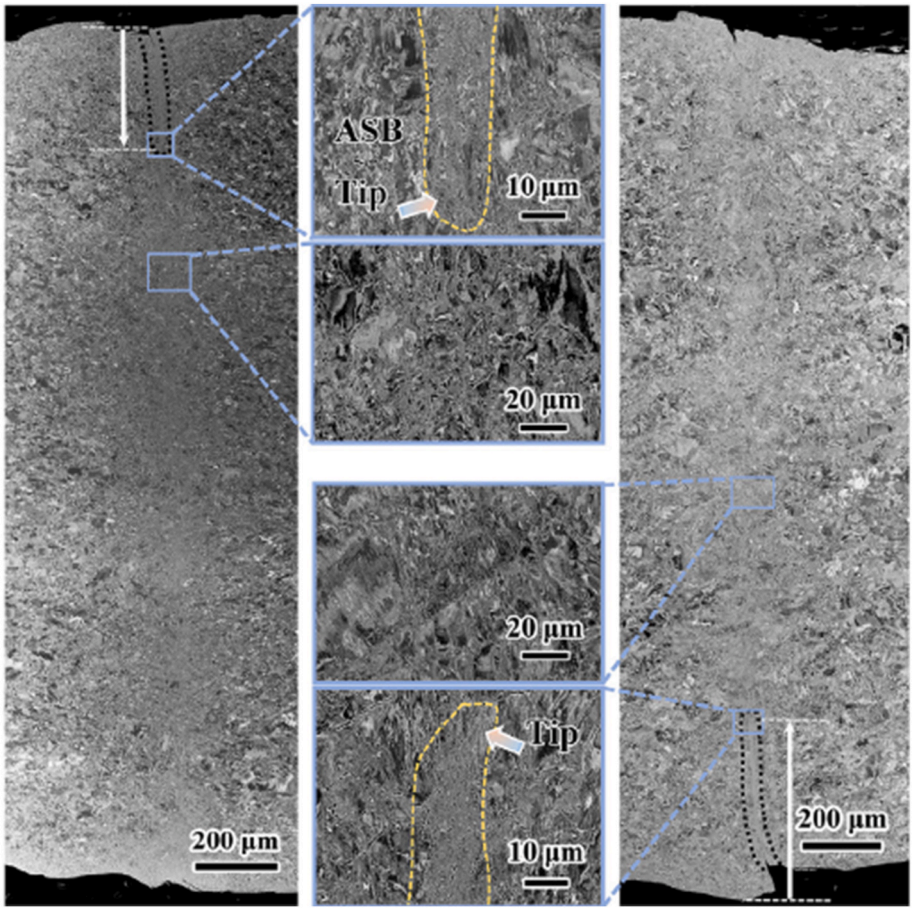

Fig. 28. BSE images showing the evolution of ASB in gradient $NiFeCr_{0.9}Al_{0.5}V_{0.2}$ MEA. Reproduced from Ref. [161].

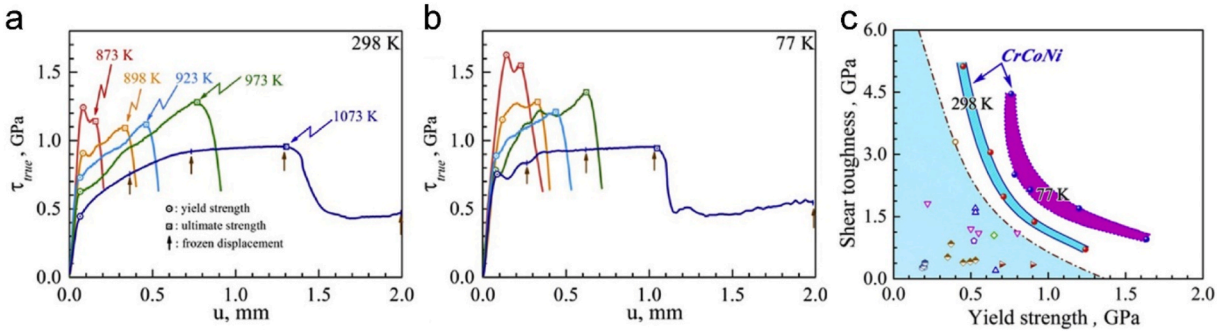

Fig. 29. Dynamic shear properties of heterogeneous grain structured MEA. Reproduced from Ref. [40].

enhanced thermal sensitivity and strain hardening rates, as evidenced by dynamic compression and tensile testing [165,166]. The experimental findings indicate a significant increase in dislocation density within the fine-grained domains, which is more pronounced compared to the coarse-grained regions. This disparity in dislocation density generates a substantial deformation gradient across the coarse- and fine-grained domains. Consequently, this deformation gradient is instrumental in the pronounced strengthening and strain hardening observed in heterogeneous-structured HEAs under dynamic compression conditions.

5.3. Dual-phase structures

Dual-phase HEAs with heterogeneous grain structures exhibit superior spall strength under high strain rates, such as those encountered in shock compression and spallation tests, ranging from 10^5 to 10^6 s^{-1} [167,168]. This enhanced performance is attributed to the shock-induced deformation twinning and phase transitions, which are identified as the predominant deformation mechanisms under shock loading conditions. Furthermore, the coherent phase boundaries, which are generated both during twinning and phase transition processes, enhance the stability of other phases, thereby contributing to the elevated spall strength observed in these heterogeneous-structured HEAs.

6. Functional behavior of heterostructured materials

Heterogeneous structures have gained widespread attention in structural materials due to their exceptional mechanical properties. Akin to the strength-ductility relationship in metals, the trade-off among essential functional properties are also prevalent, such as magnetization-

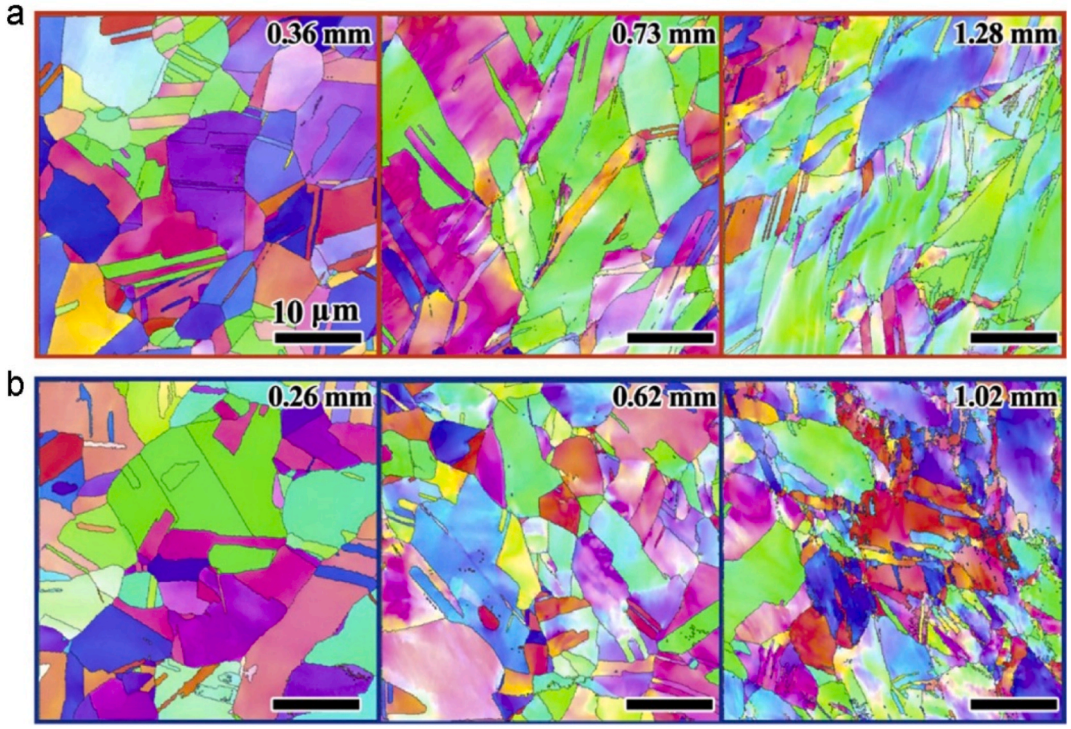

Fig. 30. The grain refinement of hetergeneous grain structured MEA during dynamic shear deformation at (a) room temperature, and (b) cryogenic temeprature. Reproduced from Ref. [40].

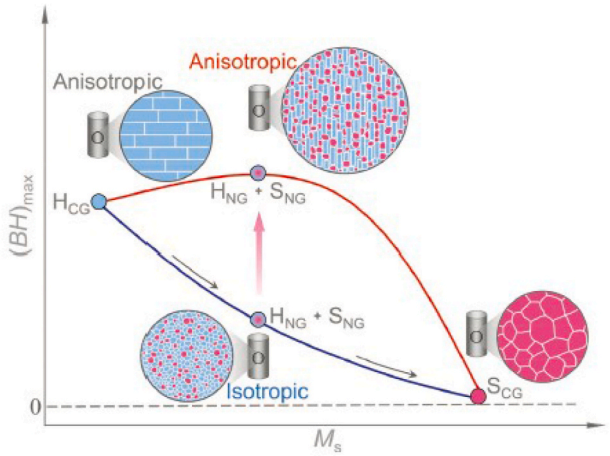

Fig. 31. Typical hysteresis loops for a permanent-magnet material. Reproduced from Ref. [169].

coercivity, electrical conductivity-Seebeck coefficient, and thermal conductivity-electrical conductivity [34]. Notably, the concept of heterostructures also holds immense potential in functional materials, enabling unprecedented functional properties such as in heterostructured magnetic materials (Fig. 31) [169], nanostructured bulk thermoelectric materials [170], and heterogeneous structures in piezoelectric materials [171]. In this context, we primarily delve into the trade-off relationship between magnetization (M_s) and coercivity (H_c) in magnetic materials.

The coercivity of a magnetic material is strongly related to the grain size, coercivity increases with decreasing grain size. Obtaining a large energy density for a permanent magnet requires both high M_s and high H_c, which is the area of its hysteresis loop in Fig. 32. Unfortunately, gaining a high M_s often results in the degradation of H_c, similar to the strength-ductility trade-off in metals, which limits the maximum energy density. A pioneering work to produce a superior synergy of magnetization-coercivity by combining hard-magnetic grains and soft magnetic grains in the bulk magnetic material was reported [172]. The hard magnetic grains have a higher H_c, and the soft-magnetic grains have higheor M_s. So the heterostructured magnetic materials perform a high energy density of the magnetism.

6.1. *Gradient nanostructured magnet*

Lou et al. [173] devised a gradient-ordered nanostructure with varying grain size to achieve directed magnetization reversal, thereby enabling $Nb_2Fe_{14}B$/α-Fe nanocomposite magnets to attain an unusual combination of high magnetization and high coercivity. In contrast, conventional $Nb_2Fe_{14}B$/α-Fe nanocomposite magnets with randomly distributed grain size tend to initiate magnetization reversal from defects and large α-Fe grains, exhibiting a random and inhomogeneous magnetic reversal process that involves the cooperative reversal of grain clusters. This magnetization reversal behavior notably decreases the H_c and compromises the squareness of the demagnetization curve, ultimately leading to a low magnetic energy product (see Fig. 33).

6.2. *Bimorphological oriented nanostructured magnet*

High-performance permanent magnets commonly consis of rare-earth compounds such as NbFeB and SmCo. Nevertheless, the soaring cost of rare earth elements restricts their widespread applications. Consequently, the development of novel permanent magnetic materials with reduced rare-earth content and nanostructuring of magnets is of utmost to meet the ever-growing demand. Li et al. introduced an innovative bimorphological anisotropic SmCo bulk nanocomposite material, comprising rod-shaped hard-magnetic SmCo grains and equiaxed soft-magnetic Fe(Co) grins, as depicted in Fig. 34a [169]. Both the SmCo grains and Fe(Co) grains possess a diameter of 10 nm. This bimorphological nanostructured magnet exhibits an unprecedented high energy product (28 MGOe), achieved with fewer rare-earth elements,

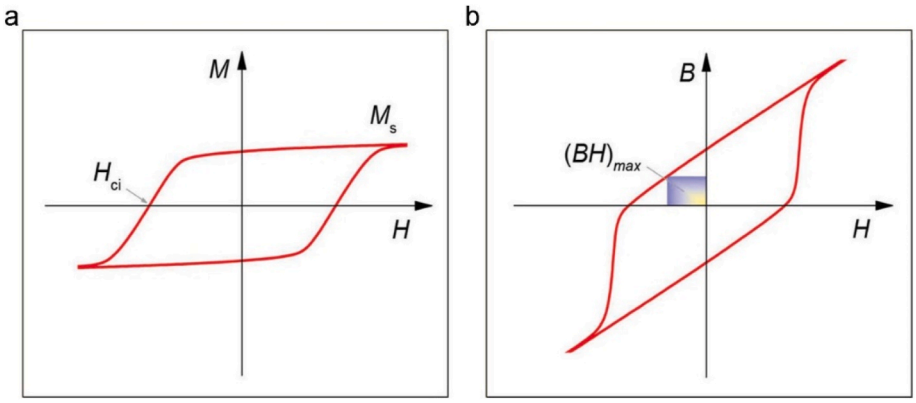

Fig. 32. Typical hysteresis loops for a permanent-magnet material. (a) The response of a magnet to an applied field (*H*) is shown in terms of its magetization *M* (a) and maganetic induction or flux density *B* (b). Reproduced from Ref. [34].

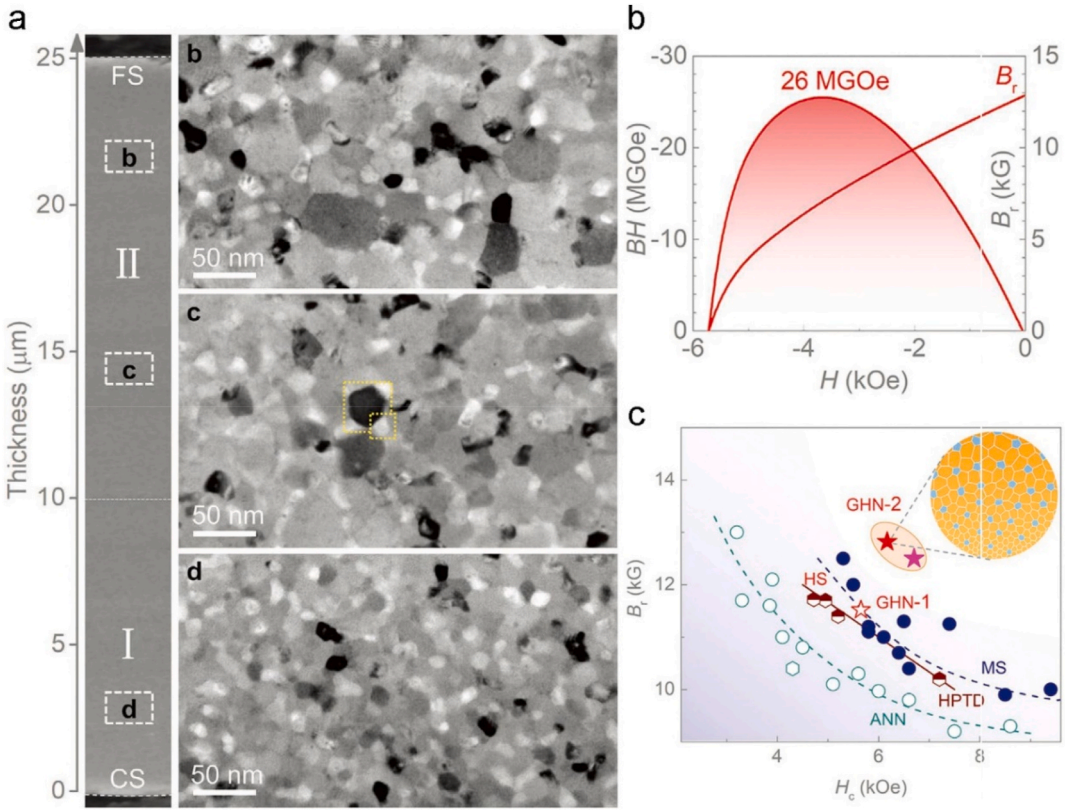

Fig. 33. Gradient nanostructures and magnetic properties of $Nb_2Fe_{14}B$/α-Fe. (a) Cross-sectional SEM and TEM images. (b) Energy products. (c) Remanence and coercivity. Reproduced from Ref. [173].

surpassing the energy product of pure rare-earth magnets, as illustrated in Fig. 34b.

6.3. *Lamella structured magnets*

Multicomponent nanostructures, which integrate multiple functional components within a single system, have the potential to generate synergistic properties through the intricate interplay between different functional components. However, these constitutent components often exhibit conflicting properties, and achieving precise control over each individual component remains a significant challenge in bulk materials. To address this, Huang et al. [174] designed a multilayer magnet composed of (SmCo + FeCo)/NbFeB through a combination of powder milling and severe plastic deformation at high pressure and high temperature, as shown in Fig. 35.

In this multicomponent layer, SmCo, a rare-earth hard magnetic compound, possesses a high magneto crystalline anisotropy and a high Curie temperature. Meanwhile, FeCo, a soft magnetic material, contributes a large saturation magnetization. NdFeB, another rare-earth hard magnetic compound, effectively combines the strengths of the SmCo's high anisotropy field and FeCo's large M_s. Remarkably, this multicomponent nanostructure achieved an exceptional energy density of 31 MGOe, as depected in Fig. 36. These groundbreaking results could pave the way for the application of this strategy to other materials systems, such as thermoelectric, multiferroic, and engineering materials, to enhance their nanostructuring capabilities.

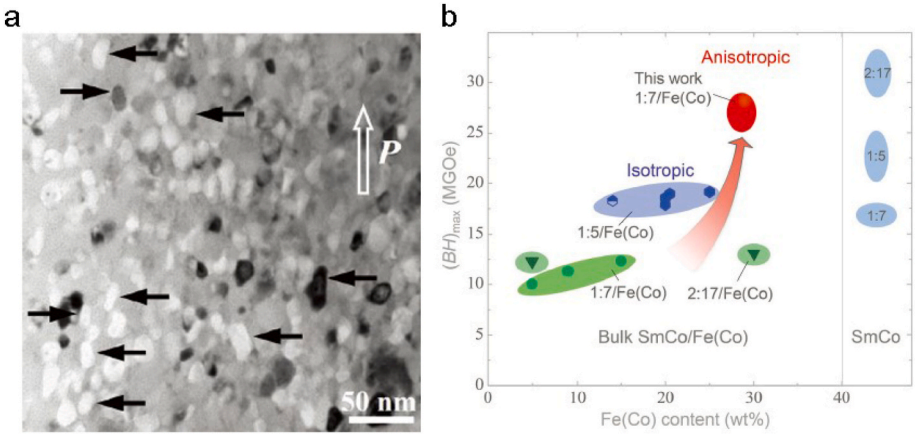

Fig. 34. Microstructure (a) and representative energy products (b) for bimorphological oriented nanostructured magnet. Reproduced from Ref. [169].

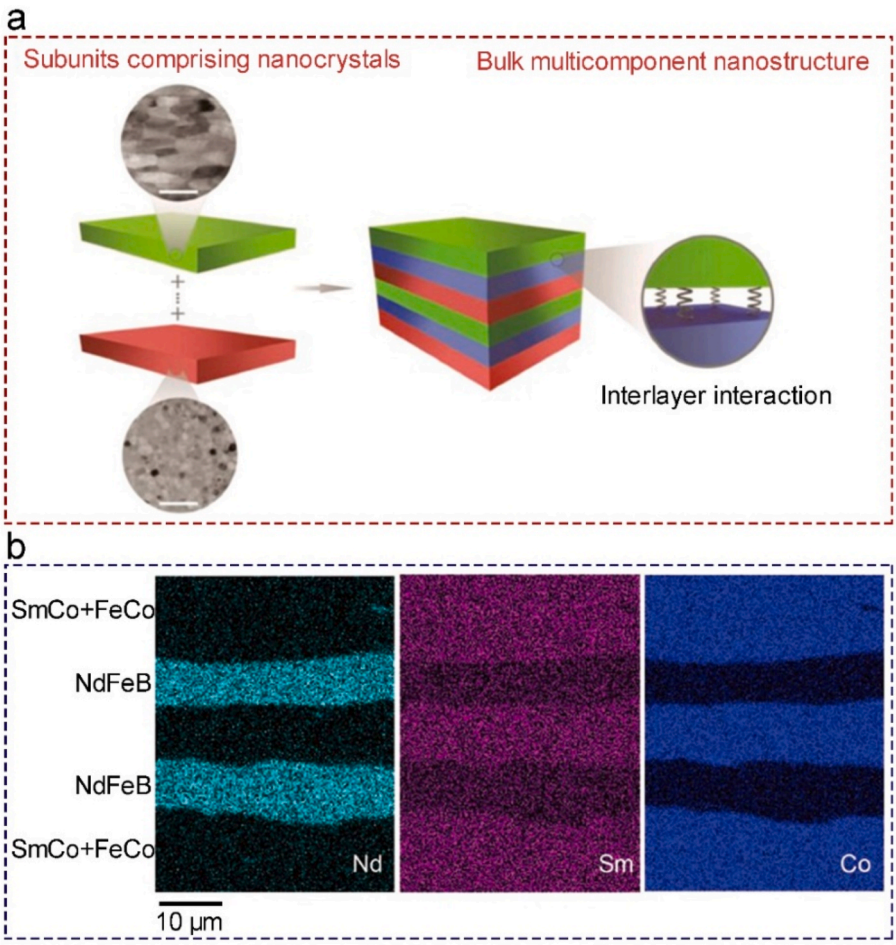

Fig. 35. Design progress (a) and structural characterization (b) of lamella structured magnet. Reproduced from Ref. [174].

6.4. *Core-shell nanostructured magnets*

Core-shell structure, also referred to as harmonic structure as defined by Ameyama [175], features coarse-grained cores embedded within a matrix of ultrafine grains (UFG) or nanograins. Inspired by this idea, Li et al. [176] designed a three-dimensional (3D) self-assembly of core-shell nanocomposite magnets, employing a sequential growth technique for the core and shell nanocrystals. This design comprises a hard-magnetic $Nd_2Fe_{14}B$ core, with a grain size of 45 nm, encased in a soft magnetic α-Fe shell, having a grain size of 13 nm, as depicted in Fig. 37. This novel core-shell nanostructured magnet boasts a record-breaking energy product, attaining the theoretical limit of isotropic $Nd_2Fe_{14}B$/s-Fe nanocomposite magnets, which stands at 25 MGOe. This precise manipulation of the nanostructured magnet underscores the fact that the core-shell architecture enables a robust exchange coupling between the hard and soft phases, even at a high soft-phase fraction of 28 %.

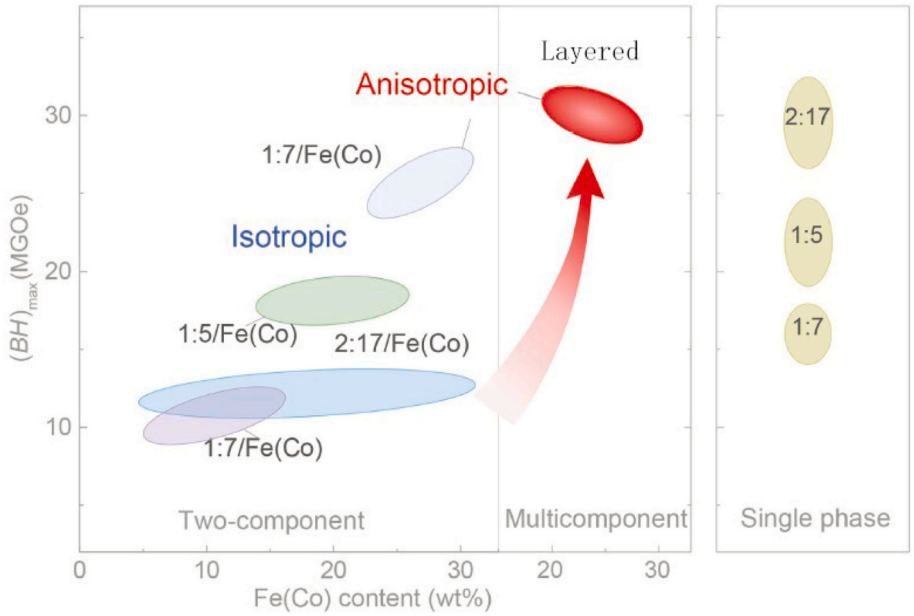

Fig. 36. Magnetic properties of the lamella structured magnet. Reproduced from Ref. [174].

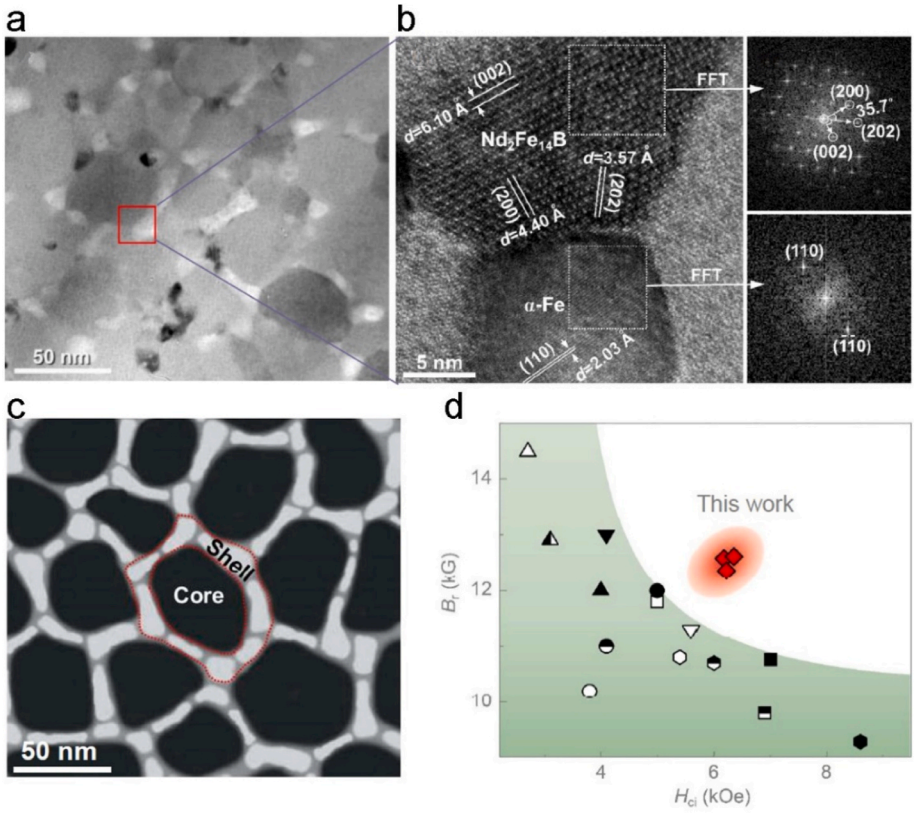

Fig. 37. Microstructures and properties of the core-shell nanostructured magnets. (a) TEM image. (b) High-resolution TEM image. (c) Schematics image. (d) Coercivity and remanence. Reproduced from Ref. [176].

7. Conclusion and perspectives

Heterogeneous structured materials exhibit a unique plastic self-coordination mechanical response, which manifests as the formation of strain gradients and subsequent generation of GNDs. The interaction of GNDs and forest dislocations, particularly their accumulation at the interfaces in heterostructured materials, indeed leads to unique additional strain hardening effects. This phenomenon not only suppresses strain localization in high-strength heterogeneous structures but also restores and enhances the plasticity and hardening of two resourced dislocations, resulting in more uniform plastic deformation across the material. This is the inherent reason for the improvement of ductility and fracture toughness in heterogeneous structured materials.

One of the pivotal challenges encountered in the realm of

heterogeneous structured materials pertains to the development of innovative design strategies for intricate heterostructures that exhibit enhanced mechanical properties and distinctive functional attributes. Currently, the fabrication of heterogeneous structured metals often relies on traditional techniques such as severe plastic deformation coupled with annealing, surface mechanical attrition treatment, and electrolytic deposition techniques. However, for the realization of highly specialized functional structures, additive manufacturing and 3D-printing technologies emerge as viable alternatives, providing unprecedented capabilities for crafting intricate heterogeneous architectures. Second, it is imperative to conduct rigorous experimental investigations alongside theoretical computational and simulation studies to gain a comprehensive understanding of the microstructural design principles underlying high-density heterogeneous interfaces and heterogeneity. The design principles and modeling of heterostructured materials are pivotal in predicting and optimizing the heterogeneity characteristics to maximize the HDI effect, which is crucial for achieving superior mechanical and functional properties that meet the demands of the industrial applications. The HDI effect is a novel scientific principle that enables heterostructured materials to exhibit unprecedented strength and ductility, surpassing the limitations predicted by traditional materials science.

CRediT authorship contribution statement

Yan Ma: Writing – original draft, Visualization. **Wei Wang:** Writing – original draft, Visualization. **Jinyan He:** Writing – original draft. **Yuntian Zhu:** Funding acquisition, Conceptualization. **Xiaolei Wu:** Funding acquisition, Conceptualization. **Fuping Yuan:** Writing – review & editing, Funding acquisition, Conceptualization.

Data availability

All data generated or analyzed during this study are included in the article and are available from the corresponding authors upon request.

Declaration of competing interest

The authors declare that they have no known competing financial interests or personal relationships that could have appeared to influence the work reported in this paper.

Acknowledgements

This research was supported by the National Key R&D Program of China [grant number 2024YFA1208004], the Strategic Priority Research Program of the Chinese Academy of Sciences [XDB0510301], the National Natural Science Foundation of China [grant numbers 52192591 and 52071326], and the Hong Kong Research Grants Council [grant GRF 11214121]. Y.Z. thanks Hong Kong Institute for Advanced Study for supporting this work at City University of Hong Kong.

Data availability

Data will be made available on request.

References

[1] Y.T. Zhu, X.L. Wu, Heterostructured materials, Prog. Mater. Sci. 131 (2023) 101019.
[2] U.G.K. Wegst, H. Bai, E. Saiz, A.P. Tomsia, R.O. Ritchie, Bioinspired structural materials, Nat. Mater. 14 (2015) 23–36.
[3] X. Li, L. Lu, J. Li, X. Zhang, H. Gao, Mechanical properties and deformation mechanisms of gradient nanostructured metals and alloys, Nat. Rev. Mater. 5 (2020) 706–723.
[4] X.L. Wu, Y.T. Zhu, Heterogeneous materials: a new class of materials with unprecedented mechanical properties, Mater. Res. Lett. 5 (2017) 527–532.
[5] Y.T. Zhu, K. Ameyama, P.M. Anderson, I.J. Beyerlein, H. Gao, H.S. Kim, E. Lavernia, S. Mathaudhu, H. Mughrabi, R.O. Ritchie, N. Tsuji, X. Zhang, X. L. Wu, Heterostructured materials: superior properties from hetero-zone interaction, Mater. Res. Lett. 9 (2021) 1–31.
[6] X.L. Wu, Y.T. Zhu, Heterostructured metallic materials: plastic deformation and strain hardening, Acta Metall. Sin. 58 (2022) 1349–1359.
[7] Y.T. Zhu, Introduction to heterostructured materials: a fast emerging field, Metall. Mater. Trans. A 52 (2021) 4715–4726.
[8] Y. Ma, M.X. Yang, F.P. Yuan, X.L. Wu, A review on heterogeneous nanostructures: a strategy for superior mechanical properties in metals, Metals 9 (2019) 598.
[9] M. Yang, Y. Pan, F. Yuan, Y. Zhu, X. Wu, Back stress strengthening and strain hardening in gradient structure, Mater. Res. Lett. 4 (2016) 145–151.
[10] Y.F. Wang, M.S. Wang, X.T. Fang, F.J. Guo, H.Q. Liu, R.O. Scattergood, C. X. Huang, Y.T. Zhu, Extra strengthening in a coarse/ultrafine grained laminate: role of gradient interfaces, Int. J. Plast. 123 (2019) 196–207.
[11] J.X. Hou, B.X. Cao, B. Xiao, Z.B. Jiao, T. Yang, Compositionally complex coherent precipitation-strengthened high-entropy alloys: a critical review, Rare Met. 41 (2022) 2002–2015.
[12] J. He, Y. Ma, D. Yan, S. Jiao, F. Yuan, X. Wu, Improving ductility by increasing fraction of interfacial zone in low C steel/304 SS laminates, Mater. Sci. Eng., A 726 (2018) 288–297.
[13] X.L. Wu, P. Jiang, L. Chen, J.F. Zhang, F.P. Yuan, Y.T. Zhu, Synergetic strengthening by gradient structure, Mater. Res. Lett. 2 (2014) 185–191.
[14] X. Zhang, J.F. Zhao, G. Kang, M. Zaiser, Geometrically necessary dislocations and related kinematic hardening in gradient grained materials: a nonlocal crystal plasticity study, Int. J. Plast. 163 (2023) 103553.
[15] S. Lu, J. Zhao, M. Huang, Z. Li, G. Kang, X. Zhang, Multiscale discrete dislocation dynamics study of gradient nano-grained materials, Int. J. Plast. 156 (2022) 103356.
[16] E. Ma, X. Wu, Tailoring heterogeneities in high-entropy alloys to promote strength-ductility synergy, Nat. Commun. 10 (2019) 5623.
[17] T.H. Fang, W.L. Li, N.R. Tao, K. Lu, Revealing extraordinary intrinsic tensile plasticity in gradient nano-grained copper, Science 331 (2011) 1587–1590.
[18] L. Lu, X. Chen, X. Huang, K. Lu, Revealing the maximum strength in nanotwinned copper, Science 323 (2009) 607–610.
[19] B.B. He, B. Hu, H.W. Yen, G.J. Cheng, Z.K. Wang, H.W. Luo, M.X. Huang, High dislocation density-induced large ductility in deformed and partitioned steels, Science 357 (2017) 1029–1032.
[20] P. Sathiyamoorthi, H.S. Kim, High-entropy alloys with heterogeneous microstructure: processing and mechanical properties, Prog. Mater. Sci. 123 (2022) 100709.
[21] L. Romero-Resendiz, M. El-Tahawy, T. Zhang, M.C. Rossi, D.M. Marulanda-Cardona, T. Yang, V. Amigo-Borras, Y. Huang, H. Mirzadeh, I.J. Beyerlein, J. C. Huang, T.G. Langdon, Y.T. Zhu, Heterostructured stainless steel: properties, current trends, and future perspectives, Mater. Sci. Eng. R 150 (2022) 100691.
[22] J.X. Hou, S.F. Liu, B.X. Cao, J.H. Luan, Y.L. Zhao, Z. Chen, Q. Zhang, X.J. Liu, C. T. Liu, J.J. Kai, T. Yang, Designing nanoparticles-strengthened high-entropy alloys with simultaneously enhanced strength-ductility synergy at both room and elevated temperatures, Acta Mater. 238 (2022) 118216.
[23] L. Chen, T. Cao, R. Wei, K. Tang, C. Xin, F. Jiang, J. Sun, Gradient structure design to strengthen carbon interstitial $Fe_{40}Mn_{40}Co_{10}Cr_{10}$ high entropy alloys, Mater. Sci. Eng., A 772 (2020) 138661.
[24] W.-L. Hsu, C.-W. Tsai, A.-C. Yeh, J.-W. Yeh, Clarifying the four core effects of high-entropy materials, Nat. Rev. Chem 8 (2024) 471–485.
[25] E.P. George, D. Raabe, R.O. Ritchie, High-entropy alloys, Nat. Rev. Mater. 4 (2019) 515–534.
[26] B. Cantor, I.T.H. Chang, P. Knight, A.J.B. Vincent, Microstructural development in equiatomic multicomponent alloys, Mater. Sci. Eng., A 375 (2004) 213–218.
[27] J.W. Yeh, S.K. Chen, S.J. Lin, J.Y. Gan, T.S. Chin, T.T. Shun, C.H. Tsau, S. Y. Chang, Nanostructured high-entropy alloys with multiple principal elements: novel alloy design concepts and outcomes, Adv. Eng. Mater. 6 (2004) 299–303.
[28] P.K. Huang, J.W. Yeh, T.T. Shun, S.K. Chen, Multi-principal-element alloys with improved oxidation and wear resistance for thermal spray coating, Adv. Eng. Mater. 6 (2004) 74–78.
[29] E.P. George, W.A. Curtin, C.C. Tasan, High entropy alloys: a focused review of mechanical properties and deformation mechanisms, Acta Mater. 188 (2020) 435–474.
[30] Q. Ding, Y. Zhang, X. Chen, X. Fu, D. Chen, S. Chen, L. Gu, F. Wei, H. Bei, Y. Gao, M. Wen, J. Li, Z. Zhang, T. Zhu, R.O. Ritchie, Q. Yu, Tuning element distribution, structure and properties by composition in high-entropy alloys, Nature 574 (2019) 223–227.
[31] S.S. Sohn, A.K. da Silva, Y. Ikeda, F. Koermann, W. Lu, W.S. Choi, B. Gault, D. Ponge, J. Neugebauer, D. Raabe, Ultrastrong medium-entropy single-phase alloys designed via severe lattice distortion, Adv. Mater. 31 (2019) 1807142.
[32] J.Y. He, Y. Ma, H.X. Li, S.Z. Ma, X.G. Zhang, F.P. Yuan, J.C.C. Huang, Plastic deformation capacity obtained by the process of strain delocalization in $Hf_{0.5}Nb_{0.5}Ta_{0.5}Ti_{1.5}Zr$ multi-principal-element alloy, Intermetallics 164 (2024) 108119.
[33] C. Baruffi, M. Ghazisaeidi, D. Rodney, W.A. Curtin, Equilibrium versus non-equilibrium stacking fault widths in NiCoCr, Scripta Mater. 235 (2023) 115536.
[34] X. Zhang, Heterostructures: new opportunities for functional materials, Mater. Res. Lett. 8 (2020) 49–59.
[35] Z. Cheng, H. Zhou, Q. Lu, H. Gao, L. Lu, Extra strengthening and work hardening in gradient nanotwinned metals, Science 362 (2018) 559–565.
[36] S. Qin, M. Yang, P. Jiang, J. Wang, X. Wu, H. Zhou, F. Yuan, Designing structures with combined gradients of grain size and precipitation in high entropy alloys for simultaneous improvement of strength and ductility, Acta Mater. 230 (2022) 117847.

[37] Z. Cheng, L. Bu, Y. Zhang, H. Wu, T. Zhu, H. Gao, L. Lu, Unraveling the origin of extra strengthening in gradient nanotwinned metals, Proc. Natl. Acad. Sci. U.S.A. 119 (2022) e2116808119.
[38] X. Wu, P. Jiang, L. Chen, F. Yuan, Y.T. Zhu, Extraordinary strain hardening by gradient structure, Proc. Natl. Acad. Sci. U.S.A. 111 (2014) 7197–7201.
[39] M. Yang, D. Yan, F. Yuan, P. Jiang, E. Ma, X. Wu, Dynamically reinforced heterogeneous grain structure prolongs ductility in a medium-entropy alloy with gigapascal yield strength, Proc. Natl. Acad. Sci. U.S.A. 115 (2018) 7224–7229.
[40] Y. Ma, F. Yuan, M. Yang, P. Jiang, E. Ma, X. Wu, Dynamic shear deformation of a CrCoNi medium-entropy alloy with heterogeneous grain structures, Acta Mater. 148 (2018) 407–418.
[41] J.X. Hou, Y. Tan, S.F. Liu, J.Y. Zhang, W.C. Xiao, H.J. Kong, Q. Li, B.X. Cao, J. H. Luan, Y.L. Zhao, J.J. Kai, T. Yang, Designing nanoparticles-strengthened high-entropy alloys with simultaneously enhanced strength-ductility synergy at both room and elevated temperatures, Acta Mater. 238 (2022) 118216.
[42] C. Zhang, C. Zhu, T. Harrington, K. Vecchio, Design of non-equiatomic high entropy alloys with heterogeneous lamella structure towards strength-ductility synergy, Scripta Mater. 154 (2018) 78–82.
[43] X. Wu, M. Yang, F. Yuan, G. Wu, Y. Wei, X. Huang, Y. Zhu, Heterogeneous lamella structure unites ultrafine-grain strength with coarse-grain ductility, Proc. Natl. Acad. Sci. U.S.A. 112 (2015) 14501–14505.
[44] J.Y. He, F.P. Yuan, M.X. Yang, L.L. Zhou, S.H. Jiao, X.L. Wu, Exceptional tensile properties under cryogenic temperature in heterogeneous laminates induced by non-uniform martensite transformation and strain delocalization, Mater. Sci. Eng., A 791 (2020) 139780.
[45] Y.K. Liu, G.H. Qin, W. Wang, Y. Ma, M.X. Yang, S.H. Jiao, X.L. Wu, F.P. Yuan, Effects of layer thickness on deformation-induced martensite transformation and tensile behaviors in a multilayer laminate, J. Mater. Res. Technol. 25 (2023) 5340–5351.
[46] C.X. Huang, Y.F. Wang, X.L. Ma, S. Yin, H.W. Hoeppel, M. Goeken, X.L. Wu, H. J. Gao, Y.T. Zhu, Interface affected zone for optimal strength and ductility in heterogeneous laminate, Mater. Today 21 (2018) 713–719.
[47] S.K. Vajpai, M. Ota, Z. Zhang, K. Ameyama, Three-dimensionally gradient harmonic structure design: an integrated approach for high performance structural materials, Mater. Res. Lett. 4 (2016) 191–197.
[48] G. Li, M. Liu, S. Lyu, M. Nakatani, R. Zheng, C. Ma, Q. Li, K. Ameyama, Simultaneously enhanced strength and strain hardening capacity in FeMnCoCr high-entropy alloy via harmonic structure design, Scripta Mater. 191 (2021) 196–201.
[49] K. Ameyama, F. Cazes, H. Couque, G. Dirras, S. Kikuchi, J. Li, F. Mompiou, K. Mondal, D. Orlov, B. Sharma, D. Tingaud, S.K. Vajpai, Harmonic structure, a promising microstructure design, Mater. Res. Lett. 10 (2022) 440–471.
[50] Z. Li, K.G. Pradeep, Y. Deng, D. Raabe, C.C. Tasan, Metastable high-entropy dual-phase alloys overcome the strength-ductility trade-off, Nature 534 (2016) 227–230.
[51] P. Shi, R. Li, Y. Li, Y. Wen, Y. Zhong, W. Ren, Z. Shen, T. Zheng, J. Peng, X. Liang, P. Hu, N. Min, Y. Zhang, Y. Ren, P.K. Liaw, D. Raabe, Y.-D. Wang, Hierarchical crack buffering triples ductility in eutectic herringbone high-entropy alloys, Science 373 (2021) 912–918.
[52] P. Shi, Y. Zhong, Y. Li, W. Ren, T. Zheng, Z. Shen, B. Yang, J. Peng, P. Hu, Y. Zhang, P.K. Liaw, Y. Zhu, Multistage work hardening assisted by multi-type twinning in ultrafine-grained heterostructural eutectic high-entropy alloys, Mater. Today 41 (2020) 62–71.
[53] Z.H. Han, S. Liang, J. Yang, R. Wei, C.J. Zhang, A superior combination of strength-ductility in CoCrFeNiMn high-entropy alloy induced by asymmetric rolling and subsequent annealing treatment, Mater. Char. 145 (2018) 619–626.
[54] Z.H. Wang, T.W. Zhang, E.L. Tang, R.L. Xiong, Z.M. Jiao, J.W. Qiao, Formation and deformation mechanisms in gradient nanostructured NiCoCrFe high entropy alloys upon supersonic impacts, Appl. Phys. Lett. 119 (2021) 201901.
[55] Q.S. Pan, L.X. Zhang, R. Feng, Q.H. Lu, K. An, A.C. Chuang, J.D. Poplawsky, P. K. Liaw, L. Lu, Gradient cell-structured high-entropy alloy with exceptional strength and ductility, Science 374 (2021) 984–989.
[56] Q.S. Pan, M.X. Yang, R. Feng, A.C. Chuang, K. An, P.K. Liaw, X.L. Wu, N.R. Tao, L. Lu, Atomic faulting induced exceptional cryogenic strain hardening in gradient cell-structured alloy, Science 382 (2023) 185–190.
[57] S. Qin, M.X. Yang, Y.K. Liu, P. Jiang, J.T. Fan, F.P. Yuan, X.L. Wu, Superior dynamic shear properties and deformation mechanisms in a high entropy alloy with dual heterogeneous structures, J. Mater. Res. Technol. 19 (2022) 3287–3301.
[58] Y.M. Wang, M.W. Chen, F.H. Zhou, E. Ma, High tensile ductility in a nanostructured metal, Nature 419 (2002) 912–915.
[59] Y.H. Zhao, T. Topping, J.F. Bingert, J.J. Thornton, A.M. Dangelewicz, Y. Li, W. Liu, Y.T. Zhu, Y.Z. Zhou, E.L. Lavernia, High tensile ductility and strength in bulk nanostructured nickel, Adv. Mater. 20 (2008) 3028–3033.
[60] A. Pandey, S. Birla, D.P. Mondal, S. Das, V.A.N. Ch, Compressive deformation behavior and strain rate sensitivity of Alcenosphere hybrid foam with mono-modal, bi-modal and tri-modal cenosphere size distribution, Mater. Char. 144 (2018) 563–574.
[61] J. Majimel, G. Molénat, M.J. Casanove, D. Schuster, A. Denquin, G. Lapasset, Investigation of the evolution of hardening precipitates during thermal exposure or creep of a 2650 aluminium alloy, Scripta Mater. 46 (2002) 113–119.
[62] Y.H. Zhao, T. Topping, Y. Li, E.J. Lavernia, Strength and ductility of Bi-modal Cu, Adv. Eng. Mater. 13 (2011) 865–871.
[63] W.G. Zhu, J. Lei, Z.X. Zhang, Q.Y. Sun, W. Chen, L. Xiao, J. Sun, Microstructural dependence of strength and ductility in a novel high strength β titanium alloy with Bi-modal structure, Mater. Sci. Eng., A 762 (2019) 138086.
[64] S. Hémery, P. Villechaise, In situ EBSD investigation of deformation processes and strain partitioning in bi-modal Ti-6Al-4V using lattice rotations, Acta Mater. 171 (2019) 261–274.
[65] T. Sakai, A. Belyakov, R. Kaibyshev, H. Miura, J.J. Jonas, Dynamic and post-dynamic recrystallization under hot, cold and severe plastic deformation conditions, Prog. Mater. Sci. 60 (2014) 130–207.
[66] D. Ponge, G. Gottstein, Necklace formation during dynamic recrystallization: mechanisms and impact on flow behavior, Acta Mater. 46 (1998) 69–80.
[67] X.H. Du, W.P. Li, H.T. Chang, T. Yang, G.S. Duan, B.L. Wu, J.C. Huang, F.R. Chen, C.T. Liu, W.S. Chuang, Y. Lu, M.L. Sui, E.W. Huang, Dual heterogeneous structures lead to ultrahigh strength and uniform ductility in a Co-Cr-Ni medium-entropy alloy, Nat. Commun. 11 (2020) 2390.
[68] S. Qin, M.X. Yang, P. Jiang, F.P. Yuan, X.L. Wu, Excellent tensile properties induced by heterogeneous grain structure and dual nanoprecipitates in high entropy alloys, Mater. Char. 186 (2022) 111779.
[69] L. Fan, T. Yang, Y.L. Zhao, J.H. Luan, G. Zhou, H. Wang, Z.B. Jiao, C.T. Liu, Ultrahigh strength and ductility in newly developed materials with coherent nanolamellar architectures, Nat. Commun. 11 (2020) 6240.
[70] R.K. Nutor, Q.P. Cao, R. Wei, Q.M. Su, G.H. Du, X.D. Wang, F.S. Li, D.X. Zhang, J. Z. Jiang, A dual-phase alloy with ultrahigh strength-ductility synergy over a wide temperature range, Sci. Adv. 7 (34) (2021) abi4404.
[71] Y. Ma, L.L. Zhou, M.X. Yang, F.P. Yuan, X.L. Wu, Ultra-high tensile strength via precipitates and enhanced martensite transformation in a FeNiAlC alloy, Mater. Sci. Eng., A 803 (2021) 140498.
[72] P.J. Shi, W.L. Ren, T.X. Zheng, Z.M. Ren, X.L. Hou, J.C. Peng, P.F. Hu, Y.F. Gao, Y. B. Zhong, P.K. Liaw, Enhanced strength-ductility synergy in ultrafine-grained eutectic high-entropy alloys by inheriting microstructural lamellae, Nat. Commun. 10 (2019) 489.
[73] C.J. Tong, Y.L. Chen, S.K. Chen, J.W. Yeh, T.T. Shun, C.H. Tsau, S.J. Lin, S. Y. Chang, Microstructure characterization of Al_xCoCrCuFeNi high-entropy alloy system with multiprincipal elements, Metall. Mater. Trans. A 36A (2005) 881–893.
[74] P.J. Shi, Y. Zhong, Y. Li, W.L. Ren, T.X. Zheng, Z. Shen, B. Yang, J.C. Peng, P. F. Hu, Y. Zhang, P.K. Liaw, Y.T. Zhu, Multistage work hardening assisted by multi-type twinning in ultrafine-grained heterostructural eutectic high-entropy alloys, Mater. Today 41 (2020) 62–71.
[75] Y.P. Lu, X.Z. Gao, L. Jiang, Z.N. Chen, T.M. Wang, J.C. Jie, H.J. Kang, Y.B. Zhang, S. Guo, H.H. Ruan, Y.H. Zhao, Z.Q. Cao, T.J. Li, Directly cast bulk eutectic and near-eutectic high entropy alloys with balanced strength and ductility in a wide temperature range, Acta Mater. 124 (2017) 143–150.
[76] Y. Zhang, T.T. Zuo, Z. Tang, M.C. Gao, K.A. Dahmen, P.K. Liaw, Z.P. Lu, Microstructures and properties of high-entropy alloys, Prog. Mater. Sci. 61 (2014) 1–93.
[77] E.P. George, R.O. Ritchie, High-entropy materials, MRS Bull. 47 (2022) 145–150.
[78] F. He, Z.J. Wang, Q.F. Wu, J.J. Li, J.C. Wang, C.T. Liu, Phase separation of metastable CoCrFeNi high entropy alloy at intermediate temperatures, Scripta Mater. 126 (2017) 15–19.
[79] X.F. Chen, Q. Wang, Z.Y. Cheng, M.L. Zhu, H. Zhou, P. Jiang, L.L. Zhou, Q.Q. Xue, F.P. Yuan, J. Zhu, X.L. Wu, E. Ma, Direct observation of chemical short-range order in a medium-entropy alloy, Nature 592 (2021) 712–715.
[80] E. Ma, C. Liu, Chemical inhomogeneities in high-entropy alloys help mitigate the strength-ductility trade-off, Prog. Mater. Sci. 143 (2024) 101252.
[81] S. Moniri, Y. Yang, J. Ding, Y.K. Yuan, J.H. Zhou, L. Yang, F. Zhu, Y.X. Liao, Y. G. Yao, L.B. Hu, P. Ercius, J.W. Miao, Three-dimensional atomic structure and local chemical order of medium- and high-entropy nanoalloys, Nature 624 (2023) 564–568.
[82] A. Naghdi, F.J. Domínguez-Gutiérrez, W.Y. Huo, K. Karimi, S. Papanikolaou, Dynamic nanoindentation and short-range order in equiatomic NiCoCr medium-entropy alloy lead to novel density wave ordering, Phys. Rev. Lett. 132 (2024) 116101.
[83] J. Wang, P. Jiang, F.P. Yuan, X.L. Wu, Chemical medium-range order in a medium-entropy alloy, Nat. Commun. 13 (2022) 1021.
[84] X.L. Wu, Chemical short-range orders in high-/medium-entropy alloys, J. Mater. Sci. Technol. 147 (2023) 189–196.
[85] Z.B. An, A. Li, S.C. Mao, T. Yang, L.Y. Zhu, R. Wang, Z.X. Wu, B. Zhang, R. W. Shao, C. Jiang, B.X. Cao, C.J. Shi, Y. Ren, C. Liu, H.B. Long, J.F. Zhang, W. Li, F. He, L.G. Sun, J.B. Zhao, L.Y. Yang, X.Y. Zhou, X. Wei, Y.M. Chen, Z.G. Lu, F. Z. Ren, C.T. Liu, Z. Zhang, X.D. Han, Negative mixing enthalpy solid solutions deliver high strength and ductility, Nature 625 (2024) 697–702.
[86] X.F. Chen, F.P. Yuan, H. Zhou, X.L. Wu, Structure motif of chemical short-range order in a medium-entropy alloy, Mater. Res. Lett. 10 (2022) 149–155.
[87] J.B. Seol, J.W. Bae, J.G. Kim, H. Sung, Z.M. Li, H.H. Lee, S.H. Shim, J.H. Jang, W. S. Ko, S.I. Hong, H.S. Kim, Short-range order strengthening in boron-doped high-entropy alloys for cryogenic applications, Acta Mater. 194 (2020) 366–377.
[88] C. Zhang, C.Y. Zhu, P.H. Cao, X. Wang, F. Ye, K. Kaufmann, L. Casalena, B. E. MacDonald, X.Q. Pan, K. Vecchio, E.J. Lavernia, Aged metastable high-entropy alloys with heterogeneous lamella structure for superior strength-ductility synergy, Acta Mater. 199 (2020) 602–612.
[89] C. Zhang, C.Y. Zhu, K. Vecchio, Non-equiatomic FeNiCoAl-based high entropy alloys with multiscale heterogeneous lamella structure for strength and ductility, Mater. Sci. Eng., A 743 (2019) 361–371.
[90] X.X. Ding, J. Wang, D. Liu, C. Wang, P. Jiang, H. Qu, G.H. Liu, F.P. Yuan, X.L. Wu, Heterostructuring an equiatomic CoNiFe medium-entropy alloy for enhanced yield strength and ductility synergy, Rare Met. 41 (2022) 2894–2905.
[91] J.J. Bhattacharyya, S.R. Agnew, G. Muralidharan, Texture enhancement during grain growth of magnesium alloy AZ31B, Acta Mater. 86 (2015) 80–94.

[92] E. Ma, T. Zhu, Towards strength-ductility synergy through the design of heterogeneous nanostructures in metals, Mater. Today 20 (2017) 323–331.
[93] Y.T. Zhu, X.L. Wu, Ductility and plasticity of nanostructured metals: differences and issues, Mater, Today Nano 2 (2018) 15–20.
[94] B. Gludovatz, A. Hohenwarter, K.V.S. Thurston, H.B. Bei, Z.G. Wu, E.P. George, R. O. Ritchie, Exceptional damage-tolerance of a medium-entropy alloy CrCoNi at cryogenic temperatures, Nat. Commun. 7 (2016) 10602.
[95] Z. Cheng, L. Lu, Fundamental strengthening mechanisms of ordered gradient nanotwinned metals, Nano Res. 16 (2023) 12430–12437.
[96] Y. Zhang, Z. Cheng, T. Zhu, L. Lu, Mechanics of gradient nanostructured metals, J. Mech. Phys. Solid. 189 (2024) 105719.
[97] F.P. Yuan, D.S. Yan, J.D. Sun, L.L. Zhou, Y.T. Zhu, X.L. Wu, Ductility by shear band delocalization in the nano-layer of gradient structure, Mater. Res. Lett. 7 (2019) 12–17.
[98] W.P. Li, T.H. Chou, T. Yang, W.S. Chuang, J.C. Huang, J.H. Luan, X.K. Zhang, X. F. Huo, H.J. Kong, Q.F. He, X.H. Du, C.T. Liu, F.R. Chen, Design of ultrastrong but ductile medium-entropy alloy with controlled precipitations and heterogeneous grain structures, Appl. Mater. Res. 23 (2021) 101037.
[99] T. Yang, Y.L. Zhao, Y. Tong, Z.B. Jiao, J. Wei, J.X. Cai, X.D. Han, D. Chen, A. Hu, J.J. Kai, K. Lu, Y. Liu, C.T. Liu, Multicomponent intermetallic nanoparticles and superb mechanical behaviors of complex alloys, Science 362 (2018) 933–937.
[100] T. Yang, Y.L. Zhao, J.H. Luan, B. Han, J. Wei, J.J. Kai, C.T. Liu, Nanoparticles-strengthened high-entropy alloys for cryogenic applications showing an exceptional strength-ductility synergy, Scripta Mater. 164 (2019) 30–35.
[101] T.L. Anderson, T.L. Anderson, Fracture Mechanics: Fundamentals and Applications, CRC Press, 2005.
[102] M.E. Launey, R.O. Ritchie, On the fracture toughness of advanced materials, Adv. Mater. 21 (2009) 2103–2110.
[103] R.O. Ritchie, The conflicts between strength and toughness, Nat. Mater. 10 (2011) 817–822.
[104] G.E. Dieter, D. Bacon, Mechanical Metallurgy, McGraw-Hill, New York, 1976.
[105] Z.Z. Li, S.T. Zhao, R.O. Ritchie, M.A. Meyers, Mechanical properties of high-entropy alloys with emphasis on face-centered cubic alloys, Prog. Mater. Sci. 102 (2019) 296–345.
[106] W.D. Li, P.K. Liaw, Y.F. Gao, Fracture resistance of high entropy alloys: a review, Intermetallics 99 (2018) 69–83.
[107] X.K. Zhu, J.A. Joyce, Review of fracture toughness (G, K, J, CTOD, CTOA) testing and standardization, Eng. Fract. Mech. 85 (2012) 1–46.
[108] R.O. Ritchie, A.W. Thompson, On macroscopic and microscopic analyses for crack initiation and crack-growth toughness in ductility alloys, Metall. Trans. A 16 (1985) 233–248.
[109] A.F. Bower, Applied Mechanics of Solids, CRC Press, 2009.
[110] J. Rice, P. Paris, J. Merkle, Some further results of J-integral analysis and estimates. Progress in Flaw Growth and Fracture Toughness Testing, ASTM International, 1973.
[111] J.R. Rice, A path independent integral and the approximate analysis of strain concentration by notches and cracks, J. Appl. Mech. 35 (1968) 379–386.
[112] J.R. Rice, Some remarks on elastic crack-tip stress fields, Int. J. Solid Struct. 8 (1972) 751–758.
[113] R.O. Ritchie, Mechanisms of fatigue-crack propagation in ductile and brittle solids, Int. J. Fract. 100 (1999) 55–83.
[114] Z.J. Zhang, M.M. Mao, J.W. Wang, B. Gludovatz, Z. Zhang, S.X. Mao, E.P. George, Q. Yu, R.O. Ritchie, Nanoscale origins of the damage tolerance of the high-entropy alloy CrMnFeCoNi, Nat. Commun. 6 (2015) 6.
[115] U. Roy, H. Roy, H. Daoud, U. Glatzel, K.K. Ray, Fracture toughness and fracture micromechanism in a cast AlCoCrCuFeNi high entropy alloy system, Mater. Lett. 132 (2014) 186–189.
[116] B. Gludovatz, A. Hohenwarter, D. Catoor, E.H. Chang, E.P. George, R.O. Ritchie, A fracture-resistant high-entropy alloy for cryogenic applications, Science 345 (2014) 1153–1158.
[117] C.C. Juan, M.H. Tsai, C.W. Tsai, C.M. Lin, W.R. Wang, C.C. Yang, S.K. Chen, S. J. Lin, J.W. Yeh, Enhanced mechanical properties of HfMoTaTiZr and HfMoNbTaTiZr refractory high-entropy alloys, Intermetallics 62 (2015) 76–83.
[118] Z.J. Zhang, H.W. Sheng, Z.J. Wang, B. Gludovatz, Z. Zhang, E.P. George, Q. Yu, S. X. Mao, R.O. Ritchie, Dislocation mechanisms and 3D twin architectures generate exceptional strength-ductility-toughness combination in CrCoNi medium-entropy alloy, Nat. Commun. 8 (2017) 8.
[119] H. Zhang, Y.Z. He, Y. Pan, Enhanced hardness and fracture toughness of the laser-solidified FeCoNiCrCuTiMoAlSiB$_{0.5}$ high-entropy alloy by martensite strengthening, Scripta Mater. 69 (2013) 342–345.
[120] D. Liu, Q. Yu, S. Kabra, M. Jiang, P. Forna-Kreutzer, R.P. Zhang, M. Payne, F. Walsh, B. Gludovatz, M. Asta, A.M. Minor, E.P. George, R.O. Ritchie, Exceptional fracture toughness of CrCoNi-based medium- and high-entropy alloys at 20 kelvin, Science 378 (2022) 978–983.
[121] X.R. Liu, S.D. Zhang, H. Feng, J. Wang, P. Jiang, H.B. Li, F.P. Yuan, X.L. Wu, Outstanding fracture toughness combines gigapascal yield strength in an N-doped heterostructured medium-entropy alloy, Acta Mater. 255 (2023) 14.
[122] Y.P. Lu, H. Jiang, S. Guo, T.M. Wang, Z.Q. Cao, T.J. Li, A new strategy to design eutectic high-entropy alloys using mixing enthalpy, Intermetallics 91 (2017) 124–128.
[123] C. Ai, F. He, M. Guo, J. Zhou, Z.J. Wang, Z.W. Yuan, Y.J. Guo, Y.L. Liu, L. Liu, Alloy design, micromechanical and macromechanical properties of CoCrFeNiTa$_x$ eutectic high entropy alloys, J. Alloys Compd. 735 (2018) 2653–2662.
[124] Z.Y. Ding, Q.F. He, Q. Wang, Y. Yang, Superb strength and high plasticity in laves phase rich eutectic medium-entropy-alloy nanocomposites, Int. J. Plast. 106 (2018) 57–72.
[125] X. Gao, H. Wang, W.J. Zhao, Y. Yang, Fabrication of strong yet malleable bulk porous high entropy laves intermetallics via chemical immersion dealloying of eutectic high entropy alloys, Scripta Mater. 219 (2022) 6.
[126] D. Chung, J. Lee, Q. He, Y.K. Kim, K.R. Lim, H.S. Kim, Y. Yang, Y. Na, Hetero-deformation promoted strengthening and toughening in BCC rich eutectic and near eutectic high entropy alloys, J. Mater. Sci. Technol. 146 (2023) 1–9.
[127] D.H. Chung, X.D. Liu, Y. Yang, Fracture of sigma phase containing Co-Cr-Ni-Mo medium entropy alloys, J. Alloys Compd. 846 (2020) 10.
[128] D. Chung, Z.Y. Ding, Y. Yang, Hierarchical eutectic structure enabling superior fracture toughness and superb strength in CoCrFeNiNb$_{0.5}$ eutectic high entropy alloy at room temperature, Adv. Eng. Mater. 21 (2019) 11.
[129] N. Meena, V. Srivastava, P. Srinivas, M. Gajendra, D.S. Gowtam, A.G. Rao, N. Prabhu, Elastic-plastic fracture toughness of wrought dual-phase non-equiatomic high-entropy alloy (HEA) for structural applications, Trans. Indian Inst. Met. 76 (2023) 1741–1750.
[130] N. Meena, D.S. Gowtam, V. Srivastava, S.S. Kumar, A.G. Rao, N. Prabhu, Elastic-plastic fracture toughness of metastable, dual-phase, Fe$_{49.5}$Mn$_{30}$Co$_{10}$Cr$_{10}$C$_{0.5}$, high entropy alloy (HEA), Mater. Lett. 351 (2023) 4.
[131] Z.M. Li, C.C. Tasan, H. Springer, B. Gault, D. Raabe, Interstitial atoms enable joint twinning and transformation induced plasticity in strong and ductile high-entropy alloys, Sci. Rep. 7 (2017) 7.
[132] J. Yang, Y.H. Jo, W. An, H.S. Kim, B.J. Lee, S. Lee, H. Sung, S.S. Sohn, Effects of deformation-induced martensitic transformation on cryogenic fracture toughness for metastable Si$_8$V$_2$Fe$_{45}$Cr$_{10}$Mn$_5$Co$_{30}$ high-entropy alloy, Acta Mater. 225 (2022) 11.
[133] Y.H. Jo, J.H. Yang, W.M. Choi, K.Y. Doh, D.H. Lee, H.S. Kim, B.J. Lee, S.S. Sohn, S. Lee, Body-centered-cubic martensite and the role on room-temperature tensile properties in Si-added SiVCrMnFeCo high-entropy alloys, J. Mater. Sci. Technol. 76 (2021) 222–230.
[134] R.O. Ritchie, J.F. Knott, J.R. Rice, Relationship between critical tensile stress and fracture toughness in mild-steel, J. Mech. Phys. Solid. 21 (1973) 395–410.
[135] J. Park, K. Lee, H. Sung, Y.J. Kim, S.K. Kim, S. Kim, J-Integral fracture toughness of high-Mn steels at room and cryogenic temperatures, Metall. Mater. Trans. A 50A (2019) 2678–2689.
[136] P. Kumar, S. Huang, D.H. Cook, K. Chen, U. Ramamurty, X.P. Tan, R.O. Ritchie, A strong fracture-resistant high-entropy alloy with nano-bridged honeycomb microstructure intrinsically toughened by 3D-printing, Nat. Commun. 15 (2024) 9.
[137] P. Foti, N. Razavi, A. Fatemi, F. Berto, Multiaxial fatigue of additively manufactured metallic components: a review of the failure mechanisms and fatigue life prediction methodologies, Prog. Mater. Sci. 137 (2023) 40.
[138] J.C. Hu, X. Li, Q.C. Zhao, Y.R. Chen, K. Yang, Q.Y. Wang, An overview on fatigue of high-entropy alloys, Materials 16 (2023) 23.
[139] K. Yang, C. He, Q. Huang, Z.Y. Huang, C. Wang, Q.Y. Wang, Y.J. Liu, B. Zhong, Very high cycle fatigue behaviors of a turbine engine blade alloy at various stress ratios, Int. J. Fatig. 99 (2017) 35–43.
[140] K. Yang, Q. Huang, Q.Y. Wang, Q. Chen, Competing crack initiation behaviors of a laser additively manufactured nickel-based superalloy in high and very high cycle fatigue regimes, Int. J. Fatig. 136 (2020) 12.
[141] Q.Y. Wang, C. Bathias, N. Kawagoishi, Q. Chen, Effect of inclusion on subsurface crack initiation and gigacycle fatigue strength, Int. J. Fatig. 24 (2002) 1269–1274.
[142] B. Zhong, X.Y. Huang, W.B. Guo, H.C. Yu, Experimental study on residual fatigue life for a nickel-based powder metallurgy superalloy. International Symposium on Structural Integrity (ISSI 2010), East China Univ Science and Technology Press, Shanghai, PEOPLES R CHINA, 2010, pp. 221–226.
[143] K. Yang, Q. Huang, B. Zhong, Q.Y. Wang, Q. Chen, Y. Chen, N. Su, H.Q. Liu, Enhanced extra-long life fatigue resistance of a bimodal titanium alloy by laser shock peening, Int. J. Fatig. 141 (2020) 12.
[144] K. Yang, Q. Huang, B. Zhong, Y.J. Liu, C. He, H.Q. Liu, N. Su, Q.Y. Wang, Q. Chen, Influence of the volume content of α plus β colonies on the very high cycle fatigue behavior of a titanium alloy, Fatig. Fract. Eng. Mater. Struct. 44 (2021) 2643–2658.
[145] Z. Zhang, H. Lin, Q. Lin, G. Chen, X. Chen, Mechanoresponsive luminogen (MRL)-based real-time and visible detection method for biaxial fatigue crack propagation, Int. J. Fatig. 164 (2022) 11.
[146] S. Suresh, Fatigue of Materials, Cambridge University Press, 1998.
[147] R. Feng, Y. Rao, C.H. Liu, X. Xie, D.J. Yu, Y. Chen, M. Ghazisaeidi, T. Ungar, H. M. Wang, K. An, P.K. Liaw, Enhancing fatigue life by ductile-transformable multicomponent B2 precipitates in a high-entropy alloy, Nat. Commun. 12 (2021) 10.
[148] R.G. Li, Q.G. Xie, Y.D. Wang, W.J. Liu, M.G. Wang, G.L. Wu, X.W. Li, M.H. Zhang, Z.P. Lu, C. Geng, T. Zhu, Unraveling submicron-scale mechanical heterogeneity by three-dimensional X-ray microdiffraction, Proc. Natl. Acad. Sci. U.S.A. 115 (2018) 483–488.
[149] L.H. Shi, Z. Zhang, X. Chen, Fatigue crack growth behavior in CoCrFeMnNi high entropy alloy with harmonic structure topology, Int. J. Fatig. 172 (2023) 11.
[150] Z. Zhang, X.Y. Zhai, G. Chen, X. Chen, K. Ameyama, Enhanced synergy of strength-ductility and low-cycle fatigue resistance of high-entropy alloy through harmonic structure design, Scripta Mater. 213 (2022) 6.
[151] Z. Zhang, X.Y. Zhai, L. Anggraini, B. Zhang, Y.S. Ma, K. Ameyama, X. Chen, Low cycle fatigue behavior and deformation mechanism of core-shell heterogeneous grain structured CoCrFeMnNi high-entropy alloy, Int. J. Fatig. 182 (2024) 14.
[152] T. Leitner, S. Pillmeier, K.S. Kormout, R. Pippan, A. Hohenwarter, Simultaneous enhancement of strength and fatigue crack growth behavior of nanocrystalline steels by annealing, Scripta Mater. 139 (2017) 39–43.

[153] Y. Tang, R.X. Wang, B. Xiao, Z.R. Zhang, S. Li, J.W. Qiao, S.X. Bai, Y. Zhang, P. K. Liaw, A review on the dynamic-mechanical behaviors of high-entropy alloys, Prog. Mater. Sci. 135 (2023) 101090.
[154] A.M. Huang, S.J. Fensin, M.A. Meyers, Strain-rate effects and dynamic behavior of high entropy alloys, J. Mater. Res. Technol. 22 (2023) 307–347.
[155] Z.L. Yang, M.X. Yang, Y. Ma, L.L. Zhou, W.Q. Cheng, F.P. Yuan, X.L. Wu, Strain rate dependent shear localization and deformation mechanisms in the CrMnFeCoNi high-entropy alloy with various microstructures, Mater. Sci. Eng., A 793 (2020) 139854.
[156] F.C. Salvado, F. Teixeira-Dias, S.M. Walley, L.J. Lea, J.B. Cardoso, A review on the strain rate dependency of the dynamic viscoplastic response of FCC metals, Prog. Mater. Sci. 88 (2017) 186–231.
[157] Z.Z. Li, S.T. Zhao, S.M. Alotaibi, Y. Liu, B.F. Wang, M.A. Meyers, Adiabatic shear localization in the CrMnFeCoNi high-entropy alloy, Acta Mater. 151 (2018) 424–431.
[158] N. Yan, Z.Z. Li, Y.B. Xu, M.A. Meyers, Shear localization in metallic materials at high strain rates, Prog. Mater. Sci. 119 (2021) 100755.
[159] K. Jiang, Q. Zhang, J.G. Li, X.Y. Li, F. Zhao, B. Hou, T. Suo, Abnormal hardening and amorphization in an FCC high entropy alloy under extreme uniaxial tension, Int. J. Plast. 159 (2022) 103463.
[160] S.T. Zhao, Z.Z. Li, C.Y. Zhu, W. Yang, Z.R. Zhang, D.E.J. Armstrong, P.S. Grant, R. O. Ritchie, M.A. Meyers, Amorphization in extreme deformation of the CrMnFeCoNi high-entropy alloy, Sci. Adv. 7 (2021) eabb3108.
[161] S. Qin, M.X. Yang, P. Jiang, J. Wang, X.L. Wu, H. Zhou, F.P. Yuan, Superior dynamic shear properties by structures with dual gradients in medium entropy alloys, J. Mater. Sci. Technol. 153 (2023) 166–180.
[162] J.Y. He, F.P. Yuan, M.X. Yang, S.H. Jiao, X.L. Wu, Superior mechanical properties and deformation mechanisms of heterogeneous laminates under dynamic shear loading, Mater. Sci. Eng., A 756 (2019) 492–501.
[163] X.D. Bian, F.P. Yuan, Y.T. Zhu, X.L. Wu, Gradient structure produces superior dynamic shear properties, Mater. Res. Lett. 5 (2017) 501–507.
[164] Y. Ma, M.X. Yang, F.P. Yuan, X.L. Wu, Deformation induced hcp nano-lamella and its size effect on the strengthening in a CoCrNi medium-entropy alloy, J. Mater. Sci. Technol. 82 (2021) 122–134.
[165] J.C. Cheng, N. Li, J.Y. Huang, A.R. Cui, X.J. Zhao, Y. Cai, Q.Y. Wang, S.N. Luo, Dynamic compression responses of heterogeneous-structured CrMnFeCoNi high-entropy alloy at cryogenic temperatures, Mater. Sci. Eng., A 892 (2024) 146063.
[166] Z. Tian, T. Zhang, Z. Wang, Z. Xie, F. Fang, Dynamic tensile deformation of Al0.1Ti0.1CoCrFeNi high-entropy alloy with heterogeneous grain structure, J. Alloys Compd. 968 (2023) 172092.
[167] K. Yang, Z.D. Feng, X.J. Zhao, J.F. Li, J.Y. Huang, Phase transitions in additively manufactured high-entropy alloy Cr10Mn10Fe60Co10Ni10 induced by high strain rate compression, Scripta Mater. 221 (2022) 114955.
[168] S.P. Zhao, Z.D. Feng, L.X. Li, X.J. Zhao, L. Lu, S. Chen, N.B. Zhang, Y. Cai, S. N. Luo, Dynamic mechanical properties, deformation, and damage mechanisms of eutectic high-entropy alloy AlCoCrFeNi2.1 under plate impact, J. Mater. Sci. Technol. 134 (2023) 178–188.
[169] X.H. Li, L. Lou, W.P. Song, G.W. Huang, F.C. Hou, Q. Zhang, H.T. Zhang, J. W. Xiao, B. Wen, X.Y. Zhang, Novel bimorphological anisotropic bulk nanocomposite materials with high energy products, Adv. Mater. 29 (2017) 1606430.
[170] K. Biswas, J.Q. He, I.D. Blum, C.I. Wu, T.P. Hogan, D.N. Seidman, V.P. Dravid, M. G. Kanatzidis, High-performance bulk thermoelectrics with all-scale hierarchical architectures, Nature 489 (2012) 414–418.
[171] F. Li, D.B. Lin, Z.B. Chen, Z.X. Cheng, J.L. Wang, C.C. Li, Z. Xu, Q.W. Huang, X. Z. Liao, L.Q. Chen, T.R. Shrout, S.J. Zhang, Ultrahigh piezoelectricity in ferroelectric ceramics by design, Nat. Mater. 17 (2018) 349–354.
[172] H.T. Zhang, X.Y. Zhang, Heterostructured functional materials with ordered structures, Acta Metall. Sin. 58 (2022) 1459–1466.
[173] L. Lou, Y.Q. Li, X.H. Li, H.L. Li, W. Li, Y.X. Hua, W.X. Xia, Z.H. Zhao, H.T. Zhang, M. Yue, X.Y. Zhang, Directional magnetization reversal enables ultrahigh energy density in gradient nanostructures, Adv. Mater. 33 (2021) 2102800.
[174] G.W. Huang, X.H. Li, L. Lou, Y.X. Hua, G.J. Zhu, M. Li, H.T. Zhang, J.W. Xiao, B. Wen, M. Yue, X.Y. Zhang, Engineering bulk, layered, multicomponent nanostructures with high energy density, Small 14 (2018) 1800619.
[175] T. Sekiguchi, K. Ono, H. Fujiwara, K. Ameyama, New microstructure design for commercially pure titanium with outstanding mechanical properties by mechanical milling and hot Roll sintering, Mater. Trans. 51 (2010) 39–45.
[176] H. Li, X.H. Li, D.F. Guo, L. Lou, W. Li, X.Y. Zhang, Three-dimensional self-assembly of core/shell-like nanostructures for high-performance nanocomposite permanent magnets, Nano Lett. 16 (2016) 5631–5638.